



**Michigan  
Technological  
University**

Michigan Technological University  
**Digital Commons @ Michigan Tech**

---

Michigan Tech Publications, Part 2

---

4-2024

## Trends of Sediment Resuspension and Budget in Southern Lake Michigan Under Changing Wave Climate and Hydrodynamic Environment

Longhuan Zhu

*Michigan Technological University, lzhu7@mtu.edu*

Pengfei Xue

*Michigan Technological University, pexue@mtu.edu*

Guy Meadows

*Michigan Technological University, gmeadows@mtu.edu*

Chenfu Huang

*Michigan Technological University, chenfuh@mtu.edu*

Jianzhong Ge

*State Key Laboratory of Estuarine and Coastal Research*

*See next page for additional authors*

Follow this and additional works at: <https://digitalcommons.mtu.edu/michigantech-p2>



Part of the [Life Sciences Commons](#)

---

### Recommended Citation

Zhu, L., Xue, P., Meadows, G., Huang, C., Ge, J., Troy, C., & Wu, C. (2024). Trends of Sediment Resuspension and Budget in Southern Lake Michigan Under Changing Wave Climate and Hydrodynamic Environment.

*Journal of Geophysical Research: Oceans*, 129(4). <http://doi.org/10.1029/2023JC020180>

Retrieved from: <https://digitalcommons.mtu.edu/michigantech-p2/687>

Follow this and additional works at: <https://digitalcommons.mtu.edu/michigantech-p2>



Part of the [Life Sciences Commons](#)

---

**Authors**

Longhuan Zhu, Pengfei Xue, Guy Meadows, Chenfu Huang, Jianzhong Ge, Cary D. Troy, and Chin H. Wu

## Trends of Sediment Resuspension and Budget in Southern Lake Michigan Under Changing Wave Climate and Hydrodynamic Environment

**Key Points:**

- Mean SSC and coastal sediment loss in southern Lake Michigan accelerated with intensified waves and lake level rise in the last decade
- Coastal SSC and sediment loss decreased in the western lake but increased in the eastern lake following the changes in incident wave energy
- Basin-wide mean SSC, coastal sediment loss, wave height, wind speed, and water level in southern Lake Michigan are highly correlated

**Supporting Information:**

Supporting Information may be found in the online version of this article.

**Correspondence to:**

L. Zhu and P. Xue,  
lzhu7@mtu.edu;  
pexue@mtu.edu

**Citation:**






Zhu, L., Xue, P., Meadows, G. A., Huang, C., Ge, J., Troy, C. D., & Wu, C. H. (2024). Trends of sediment resuspension and budget in southern Lake Michigan under changing wave climate and hydrodynamic environment. *Journal of Geophysical Research: Oceans*, 129, e2023JC020180. <https://doi.org/10.1029/2023JC020180>

Received 14 JULY 2023

Accepted 13 MAR 2024

**Author Contributions:**

**Conceptualization:** Pengfei Xue  
**Formal analysis:** Longhuan Zhu, Pengfei Xue, Guy A. Meadows, Chenfu Huang, Jianzhong Ge  
**Funding acquisition:** Pengfei Xue  
**Investigation:** Pengfei Xue  
**Methodology:** Pengfei Xue, Guy A. Meadows, Chenfu Huang, Jianzhong Ge, Chin H. Wu  
**Project administration:** Pengfei Xue  
**Software:** Longhuan Zhu, Pengfei Xue, Chenfu Huang, Jianzhong Ge  
**Supervision:** Pengfei Xue

Longhuan Zhu<sup>1</sup> , Pengfei Xue<sup>1,2,3</sup> , Guy A. Meadows<sup>1</sup> , Chenfu Huang<sup>1</sup>, Jianzhong Ge<sup>4</sup> , Cary D. Troy<sup>5</sup>, and Chin H. Wu<sup>6</sup> 

<sup>1</sup>Great Lakes Research Center, Michigan Technological University, Houghton, MI, USA, <sup>2</sup>Department of Civil, Environmental and Geospatial Engineering, Michigan Technological University, Houghton, MI, USA, <sup>3</sup>Environmental Science Division, Argonne National Laboratory, Lemont, IL, USA, <sup>4</sup>State Key Laboratory of Estuarine and Coastal Research, East China Normal University, Shanghai, China, <sup>5</sup>Lyles School of Civil Engineering, Purdue University, West Lafayette, IN, USA, <sup>6</sup>Department of Civil and Environmental Engineering, University of Wisconsin-Madison, Madison, WI, USA

**Abstract** Sediment suspension and transport driven by waves and currents play a significant role in both the ecological and physical environments of large lakes. Lake Michigan has faced a rapidly increasing water level associated with intensified wind waves in the past decade. To investigate the spatiotemporal characteristics of suspended sediment concentration (SSC) and associated coastal sediment budgets in southern Lake Michigan, a 30-year (1991–2020) hindcast was performed using a coupled wave-current-sediment model (SWAN-FVCOM-CSTMS). We found that in southern Lake Michigan, the basin-wide mean SSC increased, and the coastal sediment loss accelerated dramatically, corresponding with intensified waves, currents and lake water level rises over the past decade. The basin-wide mean SSC, coastal sediment loss, wave height, wind speed, current speed, and water level in southern Lake Michigan are highly correlated. Spatially, the results reveal decreases in coastal SSC and sediment loss in the western portion of the southern basin, while the eastern sectors show an increase in both metrics. This reflects a clear shift in the wave climate and hydrodynamic environment. The alterations in long-term coastal sediment budgets imply that considerable shoreline transformations are being influenced by modifications in the wave climate. Understanding the spatiotemporal characteristics of SSC and coastal sediment budgets is crucial for strategic water resource management and coastal infrastructure planning.

**Plain Language Summary** The movement of sediment caused by waves and currents greatly impacts the health and shape of large lakes. Over the past decade, Lake Michigan's water level has been rising rapidly, associated with stronger wind waves. To understand how these changes affect the amount of sediment in the water and along the shore in southern Lake Michigan, we employed a complex model to capture sediment changes over past the 30 years (1991–2020). We found that the average amount of sediment suspended in the water and the loss of sediment along the shore both increased as the lake's water level rose and waves became more intense. These changes were strongly correlated with the height of the waves, wind speed, and water level in the lake. We also saw decreases in coastal suspended sediment concentration and sediment loss in the western portion of the southern basin, while an increase in sediment loss within its eastern sectors, reflecting a clear shift in the wave climate and hydrodynamic environment. The changes in coastal sediment over time suggest significant shoreline reshaping, driven by shifts in wave patterns and the hydrodynamic conditions. It's important to understand these changes to manage our water resources effectively and plan our coastal infrastructures wisely.

### 1. Introduction

Lake Michigan is the fifth largest lake in the world and the third largest lake in the Great Lakes by surface area. Stretching 494 km from north to south and 190 km from east to west, Lake Michigan has a 2,640 km long shoreline and is home to approximately 12 million people. The majority of the people live along the shore of southern Lake Michigan, especially in the Chicago and Milwaukee metropolitan areas. Given its dense population, this study specifically focuses on the southern portion of Lake Michigan.

© 2024 The Authors.

This is an open access article under the terms of the [Creative Commons Attribution-NonCommercial License](https://creativecommons.org/licenses/by/4.0/), which permits use, distribution and reproduction in any medium, provided the original work is properly cited and is not used for commercial purposes.

**Validation:** Longhuan Zhu,  
Chenfu Huang  
**Visualization:** Longhuan Zhu  
**Writing – original draft:** Longhuan Zhu,  
Pengfei Xue, Guy A. Meadows, Cary  
D. Troy, Chin H. Wu  
**Writing – review & editing:**  
Longhuan Zhu, Pengfei Xue, Guy  
A. Meadows, Cary D. Troy

In large lakes, sediment plays a significant role in ecosystems through sediment suspension and transport mechanisms. The sediment suspension and transport are important for the cycling of nutrients and contaminants via sediment particles (Brooks & Edgington, 1994; Chen et al., 2004; Eadie et al., 1984; Eadie & Robbins, 1987; Ji et al., 2002; Miller et al., 2016; Millie et al., 2002; Robbins & Eadie, 1991). Furthermore, an increase in suspended sediment can diminish light transmission, which in turn decreases photosynthesis by aquatic plants, negatively affecting the growth of aquatic plants as well as the dissolved oxygen levels (Berry et al., 2003; Blom et al., 1994). When the dissolved oxygen level falls below a threshold (e.g., 5 mg/L for fish), fish and other aquatic organisms cannot survive (Bozorg-Haddad et al., 2021).

Furthermore, sediment suspension and transport associated with sediment input from coastal erosion and rivers influence the sediment budget within a region of interest. An imbalance of the sediment budget results in erosion or deposition, leading to morphological changes (Amoudry & Souza, 2011; Rosati, 2005). Long-term imbalance of the sediment budget in the nearshore and surf zone may also impact beach safety and reshape the shoreline. Thus, understanding sediment transport and budget is fundamental for coastal nourishment and coastal protection. As more and more people are relocating to the coastal areas, integrating sediment budget considerations into coastal management and planning becomes increasingly critical.

Sediment suspension and transport are primarily driven by waves and currents (Grant & Madsen, 1979; Mei et al., 1997; Miles et al., 2013). In deep water, the action of water waves cannot reach the bottom, therefore, large sediment suspension is usually initiated in shallow coastal waters. The suspended sediment is then transported alongshore and offshore, associated with flow advection and diffusion. This region of significant transport can be about 10 km wide and over 100 km long along the coast of southern Lake Michigan (Eadie et al., 1996; Lee et al., 2007). In Lake Michigan, massive sediment resuspension occurs during storm events with large waves and currents (Eadie et al., 2008; Mortimer, 1988). Since the 1980s, storms have become more frequent and ice cover has decreased with climate warming, leading to more frequent, massive sediment resuspension events (Schwab et al., 2006). During such large resuspension events, the total amount of suspended sediment is comparable to the total annual sediment input from shoreline erosion and tributaries to the entire lake (Colman & Foster, 1994; Eadie et al., 2002; Lou et al., 2000). The resuspended sediment can be transported tens or even hundreds of kilometers along the shore with redistribution throughout the lake (Hawley & Lee, 1999), resulting in enormous local erosion and deposition along the coast of southern Lake Michigan. The wave climate in Lake Michigan has changed significantly, with a decreasing wave energy trend in the western lake and an increasing trend in the eastern lake over the recent decade, coinciding with rapid lake level rises (Huang, Zhu, et al., 2021). This underscores the growing need to better understand sediment suspension and transport under changing wave climatology. Understanding the long-term change in sediment suspension and transport will benefit water resources management and coastal infrastructure construction.

The objective of this study is to investigate the spatiotemporal changes in sediment resuspension and transport in southern Lake Michigan (below the latitude of 44°N), a region noted for having one of the greatest population densities in the Great Lakes region (<https://www.britannica.com/place/Great-Lakes/Physiography>). We conducted a 30-year (1991–2020) hindcast for the entire lake using a coupled wave-current-sediment model. Following a comprehensive model validation, we examined spatiotemporal patterns of the 30-year mean sediment suspension in southern Lake Michigan. Subsequently, we explored the relationships between the long-term changes in sediment suspension and the changes in water levels, waves, and winds across both spatial and temporal dimensions. Finally, the implications of the sediment suspension and transport on the sediment budget along the coast of southern Lake Michigan are discussed.

## 2. Approach

### 2.1. Model Configuration

The wave-current-sediment processes in Lake Michigan were modeled using a 3D numerical model system, which coupled the third-generation wave spectral model, Simulating Wave Nearshore (SWAN, Booij et al., 1999), the ocean circulation model, Finite-Volume Community Ocean Model (FVCOM, Chen et al., 2003, 2006), and the sediment transport model, Community Sediment Transport Modeling System (CSTMS, Warner et al., 2008) that is integrated into FVCOM. SWAN computes random, short-crested wind-generated waves in coastal regions and inland waters. It solves the evolution equation of wave action density in space and time over frequency and wave direction considering the following physics (<https://swanmodel.sourceforge.io/features/>

features.htm): (a) wave propagation in time and space, shoaling, refraction due to current and depth, frequency shifting due to currents and non-stationary depth, (b) wave generation by wind, (c) three- and four-wave interactions, (d) white capping, bottom friction and depth-induced breaking, (e) dissipation due to aquatic vegetation, turbulent flow and viscous fluid mud, (f) wave-induced set-up, (g) propagation from laboratory up to global scales, (h) transmission through and reflection (specular and diffuse) against obstacles, (i) diffraction. With these features, SWAN has been widely applied for wave simulation for coastal oceans (Cheng et al., 2015; Dietrich et al., 2011; Huang et al., 2013; Niroomandi et al., 2018; Xie et al., 2016, 2019) and the Great Lakes (Anderson et al., 2015; Huang, Anderson, et al., 2021; Huang, Zhu, et al., 2021; Mao et al., 2016; Mao & Xia, 2017). SWAN was adapted into an unstructured-grid model and incorporated into FVCOM, forming FVCOM-SWAVE (Chen et al., 2003; Qi et al., 2009). However, its application has been constrained due to limited computational efficiency. To enhance the computational efficiency in our long-term simulation, one-way coupling with offline wave input from SWAN (Huang, Zhu, et al., 2021) was used in this study. The wave parameters including significant wave height, peak wave period, mean wave direction, mean wavelength, bottom wave orbital velocity, and bottom wave period, are passed to FVCOM with CSTMS to consider the effects of waves on currents and sediment suspension and deposition through 3D wave radiation stress and combined wave-current bottom stress in the bottom boundary layer. CSTMS was implemented into FVCOM as FVCOM-SED, which accounts for suspended and bedload transport, layered bed dynamics, and erosion/deposition actions for multiple cohesive and non-cohesive sediment classes. The vertical mixing processes and the horizontal diffusivity were calculated using the Mellor-Yamada level-2.5 (MY25) turbulence closure model (Mellor & Yamada, 1982) and the Smagorinsky numerical formulation (Smagorinsky, 1963), respectively. The FVCOM-based wave-current-sediment models have been applied for sediment transport analysis for coastal oceans (Gao et al., 2018; Ge et al., 2018; Li et al., 2022; Wu et al., 2011; Yang et al., 2022; Zhou et al., 2021) and the Great Lakes (Khazaei et al., 2021; Niu et al., 2018).

The computational domain covering the entire lake was developed using an unstructured mesh with the bathymetry data sets from the National Oceanic and Atmospheric Administration (NOAA, <https://www.ngdc.noaa.gov/mgg/greatlakes/michigan.html>). The horizontal resolution of the mesh varied from ~60 to 300 m near the coast to ~4.4 km in the central lake areas (Figure 1). In the vertical direction, the mesh was equally divided into 20 sigma layers such that the vertical resolution was about 0.05 m near the coast and less than 5 m for most offshore regions.

The sediment properties were estimated based on the alignment with previous studies and successful model calibration (Table 1). Earlier studies utilized either a single sediment size class (e.g., Lou et al., 2000) or multiple sediment size classes (e.g., Cardenas et al., 2005; Hawley et al., 2009; Khazaei et al., 2021). However, Hawley et al. (2009) pointed out that the results using two-size classes were similar to those with four-size classes. Therefore, two representative sediment classes with 15  $\mu\text{m}$  for fine sediment and 150  $\mu\text{m}$  for coarse sediment were used in this study. The fractions of fine and coarse sediment, 17% and 83% respectively, were estimated based on the sediment percentage along the coast of Lake Michigan (Eadie & Lozano, 1999; Lee et al., 2007) and further adjusted based on model calibration. Given that most of the sediment is of sand size, following the precedent set by Hawley et al. (2009) and Lou et al. (2000), the sediment is assumed to be non-cohesive. This assumption is reasonable for analyzing long-term trends on a basin-wide scale. The sediment density was estimated using the default value of 2,650  $\text{kg}/\text{m}^3$  (Soulsby, 1997), which is comparable to the estimations (2,300–2,450  $\text{kg}/\text{m}^3$ ) in Khazaei et al. (2021). The settling velocity ( $\omega$ ), surface erosion rate ( $E_0$ ), and critical shear stress for erosion ( $\tau_{ce}$ ) were calculated from sediment size and density using the formulas in Soulsby (1997), yielding  $\omega = 0.2$  mm/s,  $E_0 = 1.22 \times 10^{-6}$   $\text{kg}/\text{m}^2/\text{s}$ , and  $\tau_{ce} = 0.05$   $\text{N}/\text{m}^2$  for fine sediment, and  $\omega = 14.8$  mm/s,  $E_0 = 1.31 \times 10^{-4}$   $\text{kg}/\text{m}^2/\text{s}$ , and  $\tau_{ce} = 0.15$   $\text{N}/\text{m}^2$  for coarse sediment, where  $E_0$  was adjusted for a better comparison. In this study, we focused on the basin-scale coastal sediment resuspension and transport. The sediment sources from tributaries and shoreline erosion as well as the effects of small-scale coastal structures on sediment transport were not considered, which are further discussed in Section 4. Due to the limited data on sediment layer thickness at the basin scale, it was assumed that the bottom sediment source is unlimited, following the approach by Lou et al. (2000).

The driving forcing including downward solar radiation, wind speed and direction, air temperature, atmospheric pressure, relative humidity, and cloud cover were interpolated from the hourly data sets from Climate Forecast System Reanalysis (CFSR, Saha et al., 2010) for 1991–2010 and Climate Forecast System Version 2 (CFSv2, Saha et al., 2011) for 2011–2020, which have a spatial grid resolution of ~0.3° and ~0.2°, respectively. CFSR and CFSv2 have shown good performance for the Great Lakes regions (Huang, Anderson, et al., 2021; Huang, Zhu,



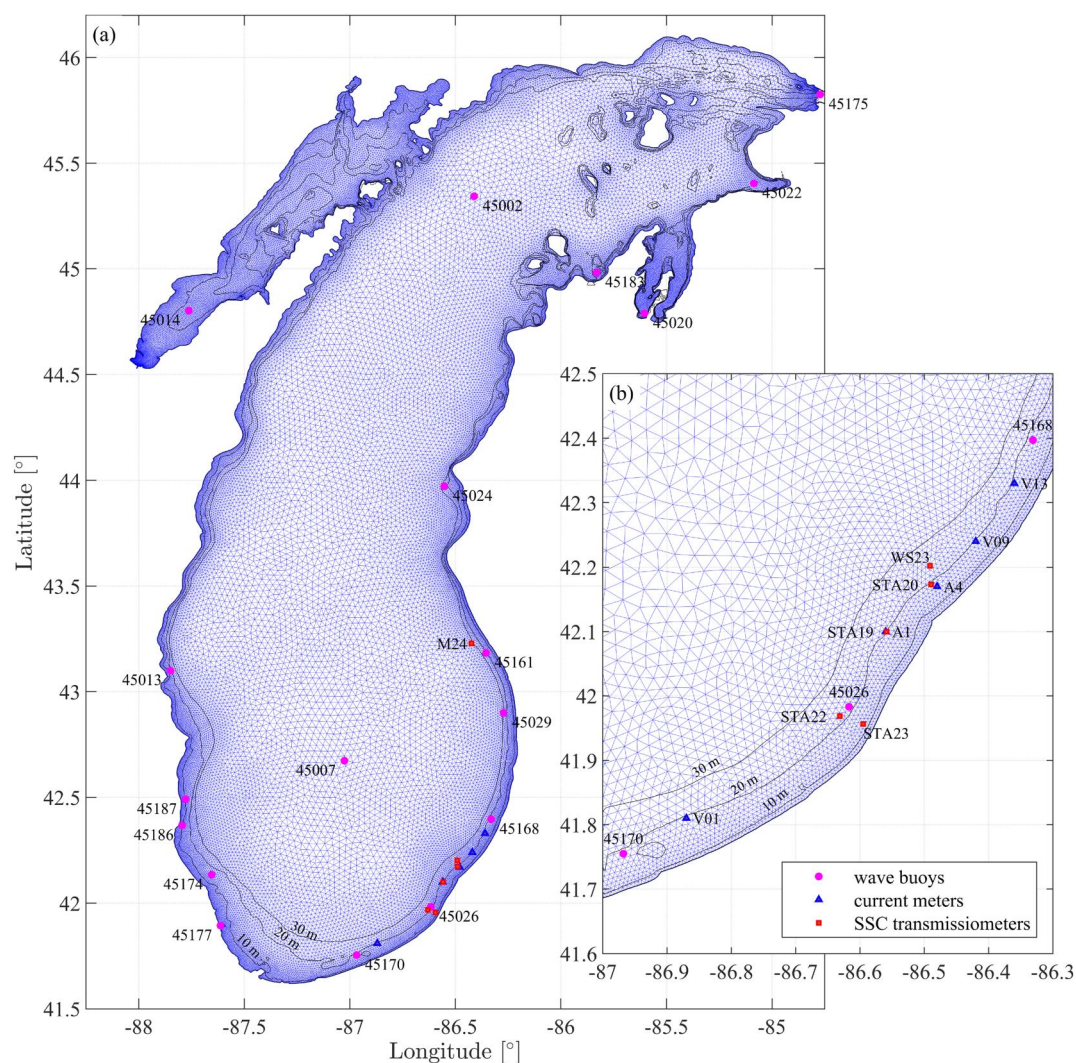


**Figure 1.** Unstructured triangular grids for FVCOM model mesh and locations for selected wave buoys (magenta circles), current meters (blue triangles), and suspended sediment concentration (SSC) transmissometers (red squares) in the coastal area for model validation in Section 2.2: (a) the entire lake and (b) zoom-in on the southeastern lake. The depth contour lines greater than 30 m are not presented.

**Table 1**  
*Sediment Parameters Used in the Model*

	Fine sediment	Coarse sediment
Mean sediment diameter $D_{50}$ [ $\mu\text{m}$ ]	15	150
Fraction	17%	83%
Sediment density $\rho_s$ [ $\text{kg}/\text{m}^3$ ]	2650	2650
Sediment settling velocity $\omega$ [ $\text{mm}/\text{s}$ ]	0.2	14.8
Surface erosion rate $E_0$ [ $\text{kg}/\text{m}^2/\text{s}$ ]	$1.22 \times 10^{-6}$	$1.31 \times 10^{-4}$
Critical shear stress for erosion $\tau_{ce}$ [ $\text{N}/\text{m}^2$ ]	0.05	0.15
Critical shear stress for deposition $\tau_d$ [ $\text{N}/\text{m}^2$ ]	0.04	0.10

et al., 2021; Jensen et al., 2012; Xue et al., 2015). The ice effects on waves were considered by masking the grid cell as land when the local ice coverage exceeds a threshold value of 30%, following Anderson et al. (2015) and Huang, Zhu, et al., 2021. The water level was updated gradually based on monthly water level data. The time steps were 3 s for FVCOM with CSTMS and 1 hr for SWAN, respectively. The model initiated at rest, with zero values for current velocity, wave height, and suspended sediment concentration. The initial temperature was set at 2°C on January 1. The bottom roughness length was set to 0.002. No open boundary conditions were employed as the whole lake was modeled, and the river influx was not considered. More details on the configurations of FVCOM and SWAN are described in Xue et al. (2017) and Huang, Zhu, et al., 2021.

## 2.2. Model Validation

The model was validated with the measured wave data from the National Data Buoy Center (NDBC, <https://www.ndbc.noaa.gov>) of NOAA (Huang, Zhu, et al., 2021), the measured current data from the project, Episodic Events–Great Lakes Experiment (EEGLE, <https://www.glerl.noaa.gov/res/projects/eegle/>), and the measured suspended sediment concentration (SSC) data from EEGLE, Lou et al. (2000), and Lee et al. (2005). Huang, Zhu, et al. (2021) have thoroughly validated the wave model that this study employs. To demonstrate the performance of the wave model, we present the comparisons in hourly significant wave height ( $H_s$ ) and peak wave period ( $T_p$ ) at 6 selected representative coastal and offshore buoys across southern Lake Michigan in 2020 in Figure 2 as an example. The difference between the calculated and measured mean values (*Bias*) and the coefficient of determination ( $R^2$ ) are used to assess the performance of the model and given by (Huang, Zhu, et al., 2021)

$$\text{Bias} = \bar{Y} - \bar{X}, \quad (1)$$

and

$$R^2 = 1 - \frac{\sum_{i=1}^N (Y_i - X_i)^2}{\sum_{i=1}^N (X_i - \bar{X})^2}, \quad (2)$$

where  $\bar{Y} = \sum_{i=1}^N Y_i/N$  is the mean of the calculated values  $Y_i$  ( $i = 1, 2, \dots, N$ ) from the model and  $\bar{X} = \sum_{i=1}^N X_i/N$  is the mean of the measured values  $X_i$  ( $i = 1, 2, \dots, N$ ) from observation with sample size of  $N$ .

The model captures the spatial and temporal characteristics of  $H_s$  very well with  $R^2$  ranging from 0.76 to 0.86 and a bias between  $-0.15$  and  $0.02$  m (Figure 2). The comparisons in  $T_p$  are reasonably well with  $R^2$  of 0.48–0.66 and a bias ranging from  $-0.18$  to  $0.46$  s (Figure 2). For certain extreme events, the model tends to underestimate the local maximum  $H_s$ . For example, the modeled largest  $H_s = 1.47$  m is less than the measured largest  $H_s = 2.98$  m on 4 August 2020, at buoy 45,174 (Figure 2f1). Overall, the model results are in good agreement with the measured data for wave comparison.

The model performance in the current simulation is demonstrated by comparing the model current velocities in the east ( $u$ ) and north ( $v$ ) directions with the observations in the southern part of Lake Michigan in 1997 (Figure 3). Additional comparisons for other years (1998, 1999, and 2000) are provided in the (Figures S1–S5 in Supporting Information S1). The model currents match well with the observations with  $R^2$  values ranging from 0.50 to 0.80 and biases less than 0.03 m/s (Figure 3). The model underestimates some large current velocities at sites A1 (Figure 3a) and V01 (Figure 3c), such as the peak current velocities on 6 December 1997. However, overall, the model and the observations generally align well.

The effectiveness of the model in simulating sediment transport is assessed through the comparison between the modeled and measured suspended sediment concentration (SSC) as illustrated in Figure 4. Though sediment models are generally known to be less precise compared to wave and hydrodynamic models, our model SSC reasonably reproduced the observed patterns, with an  $R^2$  ranging from 0.39 to 0.77 and a bias between  $-3.35$  and  $-0.19$  mg/L (Figure 4) except at the location STA20, which shows a low  $R^2$  value of 0.05 in 1998 (Figure 4e).

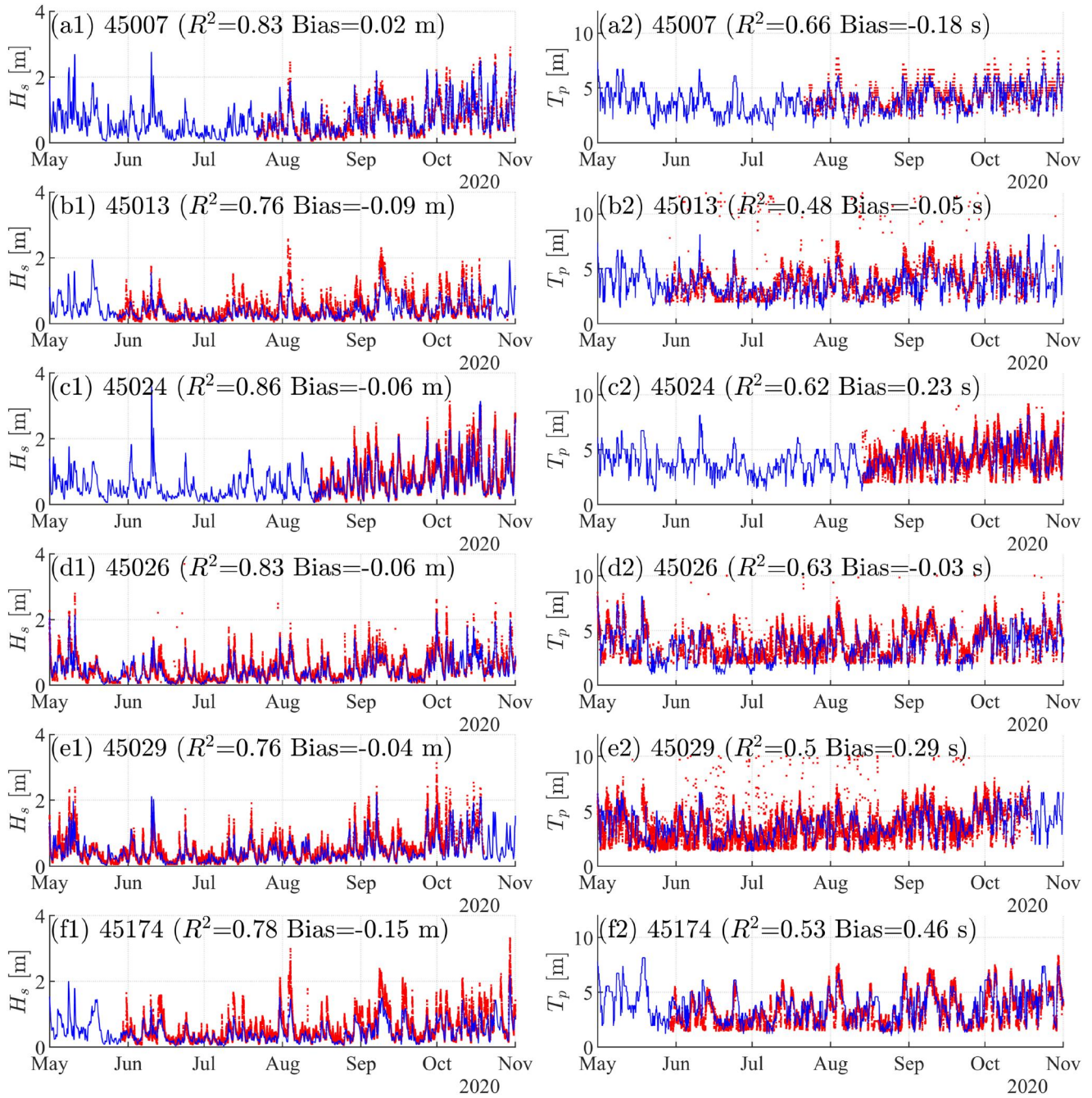


**Figure 2.** Significant wave height ( $H_s$ ) and peak period ( $T_p$ ) comparison at six representative buoys in southern Lake Michigan for the year 2020. Buoy locations are shown in Figure 1. More comparisons for more buoy stations (14 buoy stations over the whole lake) and other years (2012, 2014, 2016, 2018) are referred to Huang, Zhu, et al., 2021.

Despite this low  $R^2$  at this site, the model still captured major SSC events, such as on November 11 and 23 December 1998. In 1999, the model at this site performed relatively better, with an  $R^2$  of 0.39 (Figure 4g). Overall, there is an adequate to good agreement between the modeled SSC and the observed data. The validated model was then used to perform a 30-year hindcast from 1991 to 2020 to examine the spatiotemporal patterns of SSC in southern Lake Michigan.



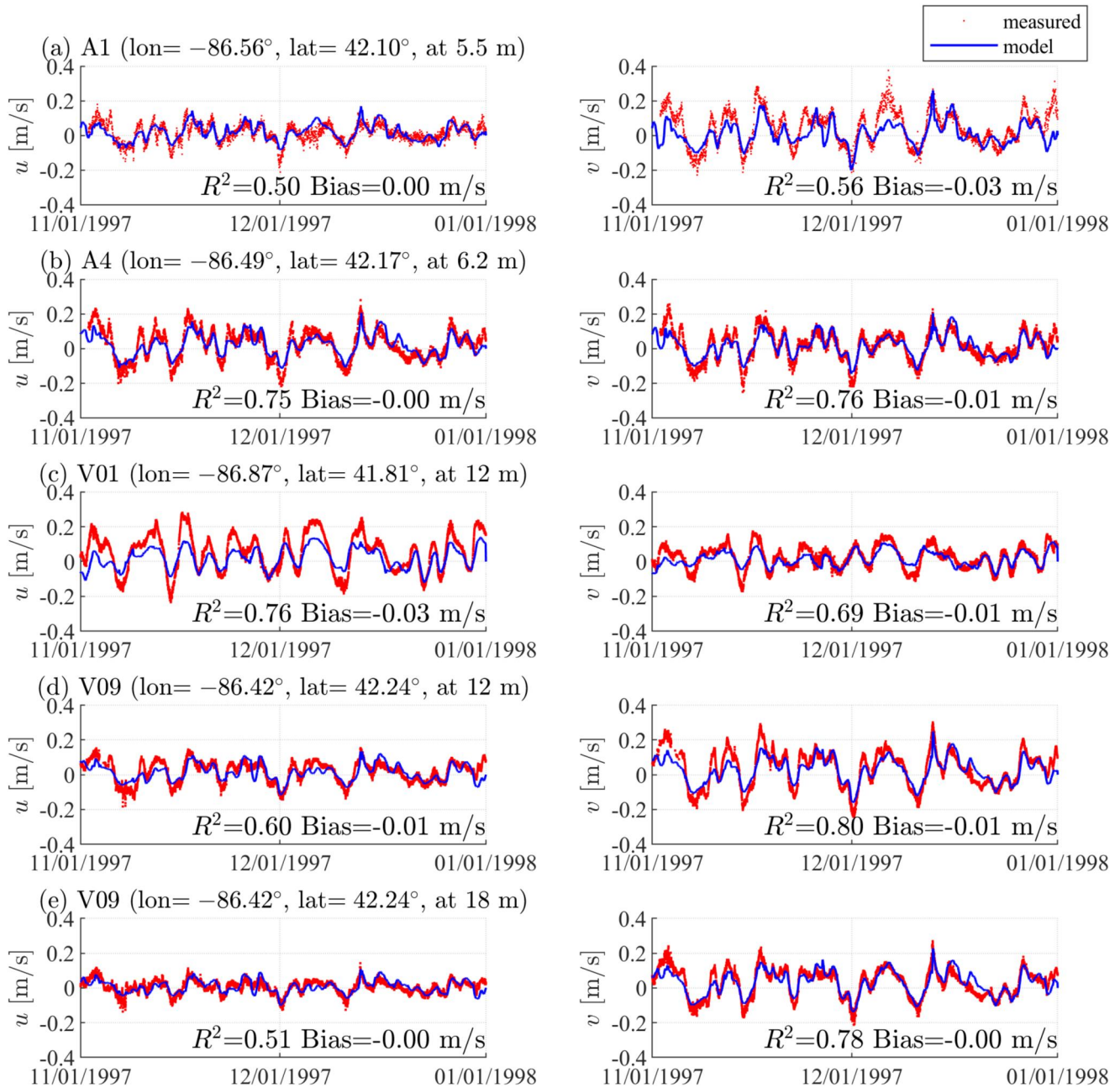


**Figure 3.** Current velocity ( $u$  positive eastward,  $v$  positive northward) comparison for the year 1997. The locations for the data are shown in Figure 1. More comparisons for other years (1998, 1999, and 2000) are shown in Figures S1–S5 in Supporting Information S1.

### 3. Results

#### 3.1. Basin-Wide Suspended Sediment Concentration (SSC) in Southern Lake Michigan

The annual basin-wide mean of depth-averaged suspended sediment concentration ( $SSC_a$ ), significant wave height ( $H_s$ ), and wind speed ( $U_{10}$ ) in southern Lake Michigan (below 44°N) over the 30 years from 1991 to 2020 is shown in Figure 5. These variables exhibited dramatic fluctuations, with the highest  $SSC_a$  occurring in 2012 and the highest  $H_s$  and  $U_{10}$  in 2013, closely preceding the strong El Niño event of 2014–2016. Over the past 30 years, the water level decreased from a high of 177.0 m in 1997 to approximately 176 m, and maintained this lower level from 2000 to 2013. It then surged rapidly to a near-record high of 177.3 m from 2014 to 2020 (Figure 5). Linear regression analysis revealed an annual upward trend in  $SSC_a$  at a rate of  $\beta = 0.0026 \pm 0.0018$  mg/L, which,

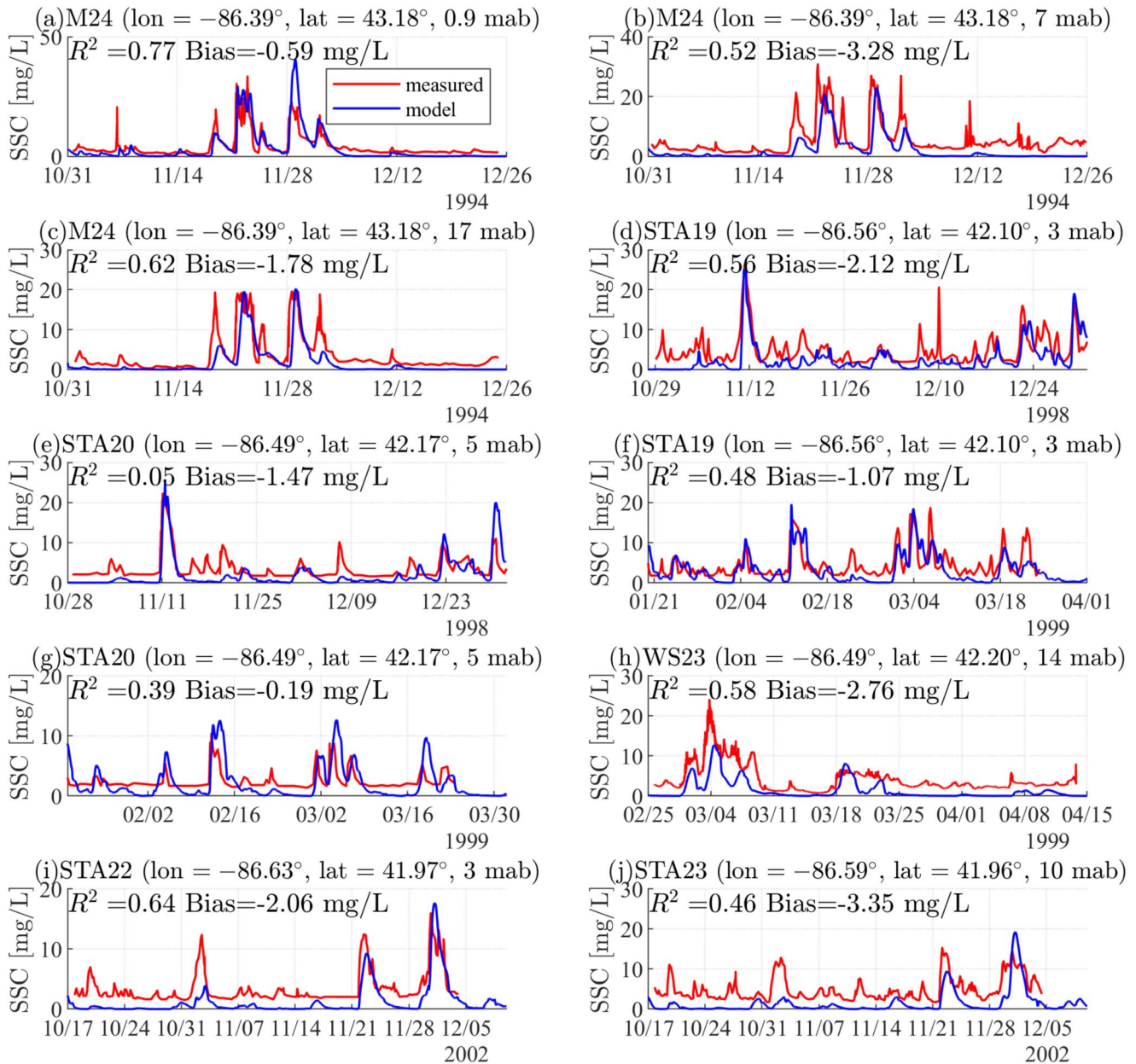


**Figure 4.** Data comparison for suspended sediment concentration (SSC) in 1994, 1998, 1999, and 2002 at different locations and water depths (mab: meters above bottom).

however, was not statistically significant with  $p = 0.17 > 0.05$ . Similarly,  $H_s$  and  $U_{10}$  also increased at rates of  $0.0017 \pm 0.0009$  m/yr and  $0.005 \pm 0.003$  m/s/yr, but these increases were also not statistically significant with  $p = 0.07$  and  $p = 0.14$ , respectively.

As there are no statistically significant linear trends for  $SSC_a$ ,  $H_s$ , and  $U_{10}$ , an alternative technique to analyze these long-term trends is to utilize moving mean methods, aiming at removing the seasonal and annual variability (Huang, Zhu, et al., 2021; Meadows et al., 1997). Following Huang, Zhu, et al. (2021), the 10-year trailing moving mean method was implemented. Figure 6 presents the 10-year trailing moving mean values of  $SSC_a$ ,  $H_s$ , and  $U_{10}$ , as well as depth-averaged mean current speed ( $U_{ca}$ ), in southern Lake Michigan, in relation to the lake water level.  $SSC_a$ , along with  $H_s$ ,  $U_{10}$ , and  $U_{ca}$  have dramatic increased since 2010, corresponding with a rise in the lake water level starting in 2013, indicating a lag of about 3 years (Figure 6). The strong correlations among  $SSC_a$ ,  $H_s$ ,  $U_{ca}$ ,

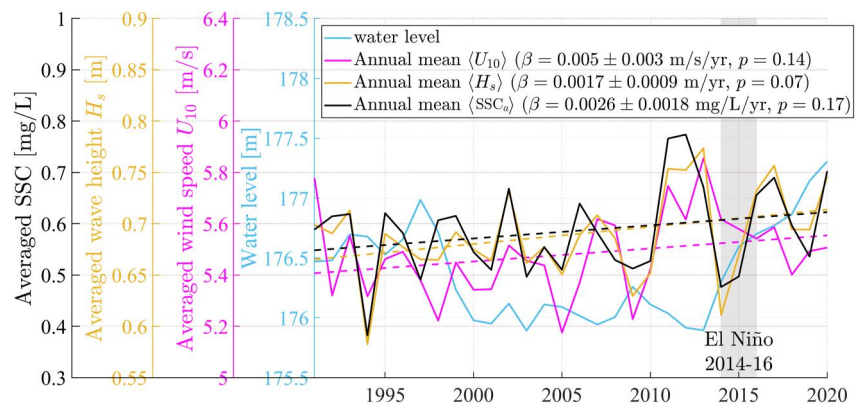


**Figure 5.** Modeled annual mean basin-wide depth-averaged suspended sediment concentration ( $SSC_a$ ), significant wave height ( $H_s$ ), and wind speed ( $U_{10}$ ) as well as the water level in southern Lake Michigan. The linear trends ( $\beta$ ) of  $U_{10}$ ,  $H_s$ , and  $SSC_a$  with standard error and  $p$ -value are shown in the legend. The shaded patch indicates the strong El Niño event 2014–16.

and  $U_{10}$  reflects the fact that the sediment resuspension is closely associated with waves and currents, which are mainly driven by wind forcing.

More importantly, the long-term changes in  $SSC_a$ ,  $H_s$ , and  $U_{10}$  are all highly correlated with water level changes, with the correlation coefficients ( $r$ ) of 0.80, 0.86, and 0.84, respectively. The long-term changes in  $U_{ca}$  also show a fairly strong correlation of 0.69 with water level, yet not as strong as the correlations of other variables with water level change. This difference is attributable to the fact that depth-averaged currents are influenced not only by surface winds but also by changes in the thermal structure, which result in density-driven circulation. Note that the high correlations do not imply the direct causal relationship between water level and  $SSC_a$ ,  $H_s$ ,  $U_{10}$ , and  $U_{ca}$ , rather, they highlight the impact of regional climate variations on these variables. Regional climate assessment showed that the frequency and intensity of storms over the Great Lakes region have increased in the past decade. Consequently, more intense storms associated with stronger winds intensified the generation and growth of waves and currents in the Great Lakes (Donelan et al., 1985; Huang, Zhu, et al., 2021; Pore, 1979), resulting in the acceleration of  $SSC_a$ . Meanwhile, the amount of precipitation has also increased (USGCRP, 2017), which, along with runoff, channel flow, and evaporation, has driven the water level rise in the Great Lakes (Deacu et al., 2012; Gronewold et al., 2021; Gronewold & Rood, 2019). Unlike the near-instant effects of storms on waves, and the resultant sediment resuspension and transport, the impact of precipitation on lake level rises may take more time, which varies from a few months to several years (Changnon, 1987; Meadows et al., 1997), due to the complexity

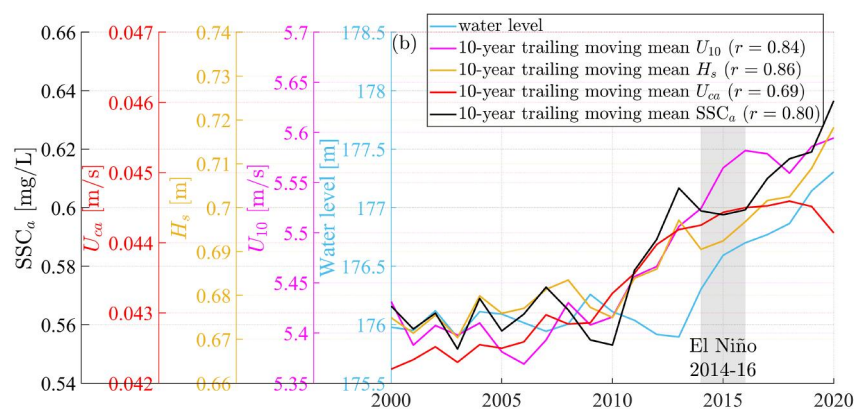


**Figure 6.** Long-term changes of 10-year trailing moving mean basin-wide depth-averaged suspended sediment concentration ( $SSC_a$ ), significant wave height ( $H_s$ ), current speed ( $U_{ca}$ ) and wind speed ( $U_{10}$ ) as well as the water level in southern Lake Michigan. The correlation coefficients ( $r$ ) with lake level are shown in the legend. The shaded patch indicates the strong El Niño event 2014–16.



of the basin-wide hydrologic cycle. Thus, increases in  $U_{10}$ ,  $H_s$ ,  $SSC_a$  and  $U_{ca}$  have preceded lake level rise by several years (Figure 6).

For the sensitivity analysis regarding the selection of the time window for the moving average, we conducted examinations using the 5-year and 7-year trailing moving averages (not shown). The results derived from these smaller time windows are less smooth than those from the 10-year trailing mean. However, all the results consistently indicate increasing trends in  $SSC_a$ ,  $H_s$ , and  $U_{10}$  after 2010, in alignment with the results derived from the 10-year trailing average.

### 3.2. Spatial Patterns of the SSC in Southern Lake Michigan

Figure 7 shows the 30-year mean of depth-averaged, surface, and bottom suspended sediment concentration (SSC). As expected, the bottom SSC is the highest, followed by the depth-averaged SSC, with the surface SSC being the lowest. In most regions with a depth of less than 20 m, SSC is significant, exceeding 1 mg/L. It is important to emphasize that these values represent the 30-year mean SSC. During individual sediment plume events, SSC can be much higher. In a few regions, significant SSC (>1 mg/L) can extend to depths of up to 30 m. This aligns with the observations that sediment resuspension occurs frequently in shallow waters, specifically those less than 30 m deep (Hawley & Lee, 1999; Lee et al., 2005). High SSC levels (>10 mg/L) are found along the shore of Sheboygan and south of Racine in the State of Wisconsin on the lake's western side. Along the shore of Illinois in the southwestern lake, the SSC levels are much higher, especially at the headland between Waukegan and Chicago. In the southeastern lake, high SSC extends along the shore from St. Joseph to Muskegon in Michigan. The SSC is also significant along the shore of Ludington in the eastern lake.

After understanding the spatial pattern of the 30-year mean SSC in southern Lake Michigan, we further investigated the spatial pattern of the long-term changes in annual SSC at 120 coastal locations (stations), situated ~5 km apart along the shore and ~2.5 km offshore (Figure 8a). Our focus was on the recent 20 years from 2000 to 2020 which encompasses a decadal low water period (2000–2013) followed by a rapid increase in water level (2014–2020) (Figure 6). Out of the 120 stations, only 22 exhibited statistically significant ( $p$ -value <0.05) linear trends in SSC (Figure 8b). In comparison, more stations showed statistically significant linear trends for  $H_s$  (27 stations),  $U_c$  (75 stations),  $U_{10}$  (96 stations), shown in Figure 8b. This is likely due to the increasing complexity of the physical processes from wind field to current and wave dynamics to sediment resuspension and transport. Among all the stations with statistically significant linear trends, the results suggest a consistent pattern: SSC decreased in the western lake and increased in the eastern lake, aligned with changes in wind, waves, and currents.

Considering the water level regime shift from the decadal low (2000–2013) to a phase of rapid increase (2014–2020), we conducted an alternative analysis to examine the spatial pattern of the changes in local SSC between these two periods (2000–2013 vs. 2014–2020) (Figure 6), where the regime shift year 2014 corresponds to the strong El Niño event 2014–16. The spatial patterns of the changes between the two periods in  $SSC_a$ ,  $SSC_s$ , and  $SSC_b$  are consistent with spatial correlation coefficients of  $r = 0.99$  and  $r = 0.98$  (Figure 8c). Moreover, the changes in  $SSC_a$  are also highly correlated with the changes in wave height, wind and currents ( $H_s$ ,  $U_{10}$ ,  $U_{cs}$ ,  $U_{ca}$ , and  $U_{cb}$ ), with all correlation coefficients  $r \geq 0.90$  (Figure 8c). The regime shift analysis further corroborates that the SSC decreased in the western lake while increasing in the eastern lake consistent with the changes in wind, waves, and currents. Sensitivity analysis for the locations at 1 and 5 km offshore are shown in Figures S6 and S7 in Supporting Information S1, and these analyses reveal similar spatial patterns.

### 3.3. Coastal Sediment Budget in Southern Lake Michigan

To explore the implications of sediment resuspension and transport on the coastal sediment budget, we divided the coast of southern Lake Michigan into 120 contiguous budget cells, each approximately ~5 km in width (offshore direction) and ~5 km in length (alongshore direction) (Figure 9a). We selected 5 km-wide budget cells because our 30-year wave simulation results showed that 70% of the lakeward edges of these budget cells were influenced by the largest 10% storm waves, which are the major drivers of large sediment resuspension. The wave effects diminish further offshore. Results from 1 km-wide and 2 km-wide budget cells are presented in Figure 9b for the purpose of sensitivity analysis. In this study, the net change in sediment budget within each cell volume was the result of sediment being transported in and out of the cell with the coastal longshore and cross-shore currents over a given period. The positive sediment budget indicates sediment gain (deposition) in the budget cell while the negative sediment budget indicates sediment loss (erosion) in the budget cell. In this study, we



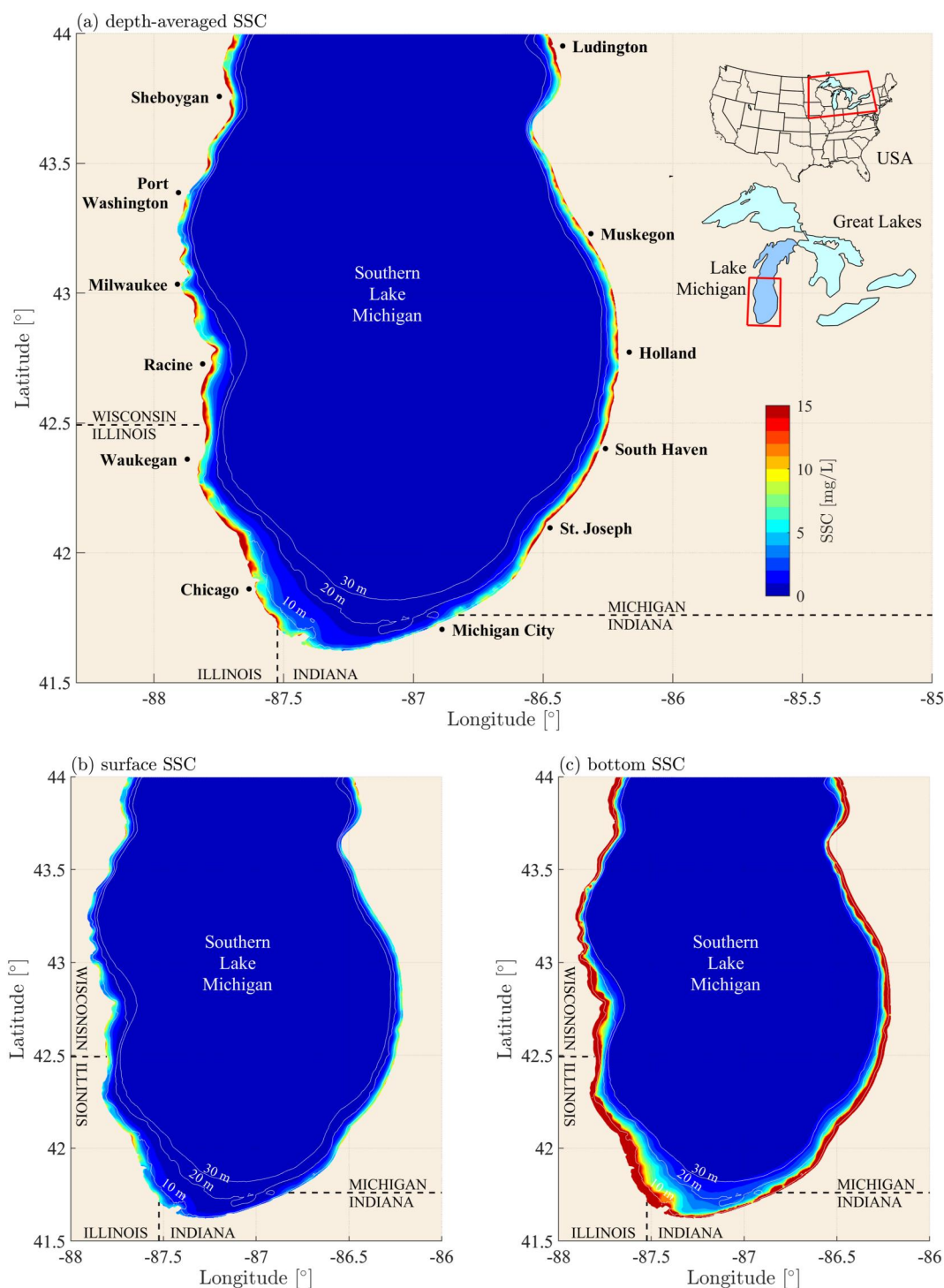


**Figure 7.** Modeled 30-year (1991–2020) mean of (a) depth-averaged, (b) surface, and (c) bottom suspended sediment concentration (SSC) in southern Lake Michigan. The depth contour lines greater than 30 m are not presented.

focused on the sediment budget changes due to sediment suspension, transport, and redistribution. The sediment input from rivers and land-based sources through shoreline erosion or bluff erosion was not considered.

The 30-year mean sediment budget in the 5 km-wide coastal regions in southern Lake Michigan is shown in Figure 9a. In the western lake, most budget cells around Sheboygan experienced sediment gain while the budget

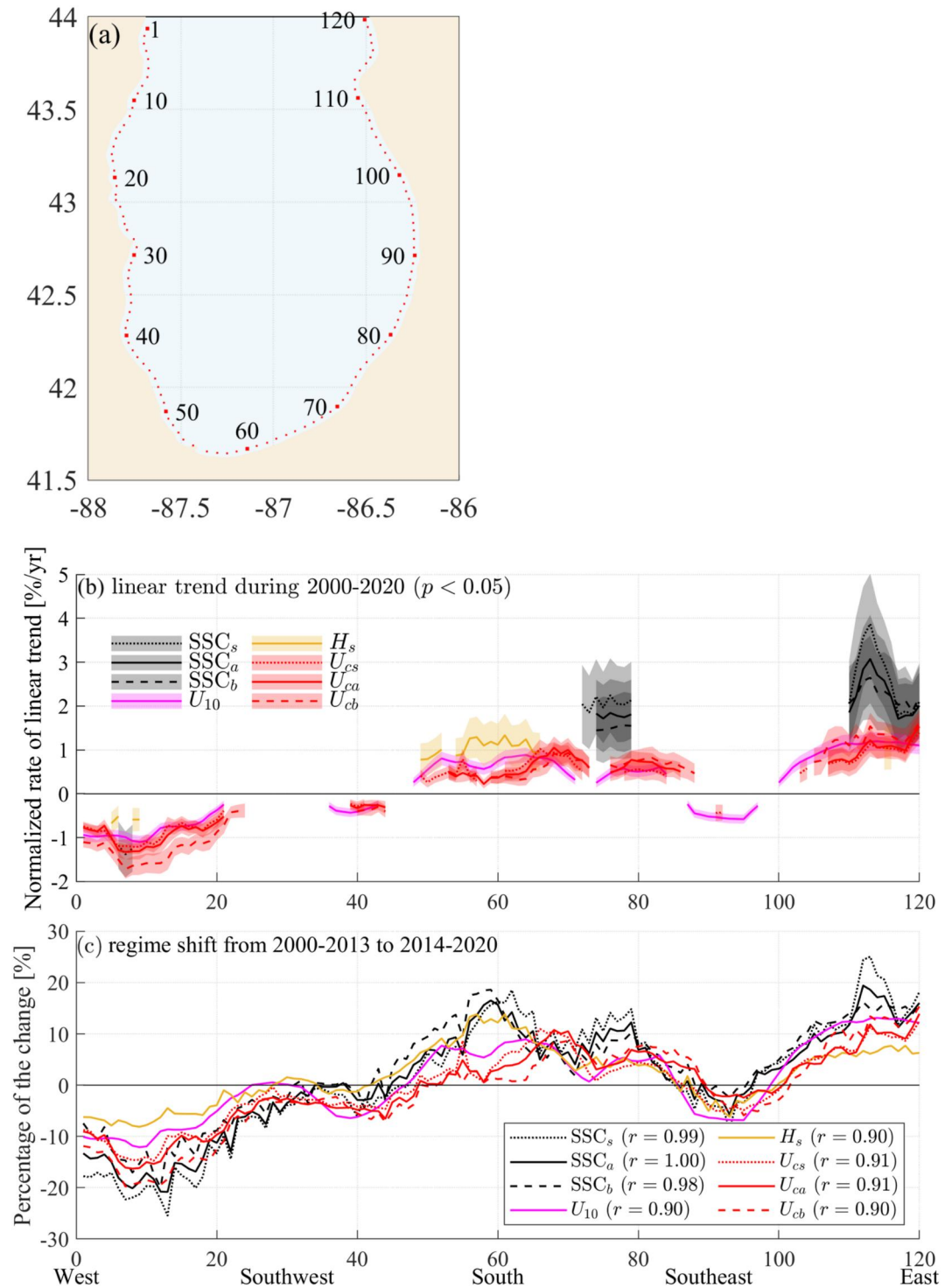


**Figure 8.** (a) Map for the selected 120 stations, which are  $\sim 5$  km apart along the shore and  $\sim 2.5$  km offshore and numbered from west to east. (b) Statistically significant ( $p$ -value  $< 0.05$ ) linear trends for annual mean  $SSC_s$ ,  $SSC_a$ ,  $SSC_b$ ,  $U_{cs}$ ,  $U_{ca}$ ,  $U_{cb}$ ,  $H_s$ , and  $U_{10}$  in the 120 coastal stations from 2000 to 2020. The surface, depth-averaged, and bottom values of suspended sediment concentration (SSC) and current speed ( $U_c$ ), are denoted by subscript  $s$ , subscript  $a$ , and subscript  $b$ . (c) The changes in the mean  $SSC_s$ ,  $SSC_a$ ,  $SSC_b$ ,  $U_{cs}$ ,  $U_{ca}$ ,  $U_{cb}$ ,  $H_s$ , and  $U_{10}$  from 2000 to 2013 with low water levels to 2014–2020 with high water levels. The correlation coefficients ( $r$ ) between the change in  $SSC_a$  change with changes in these values are shown in the legend.

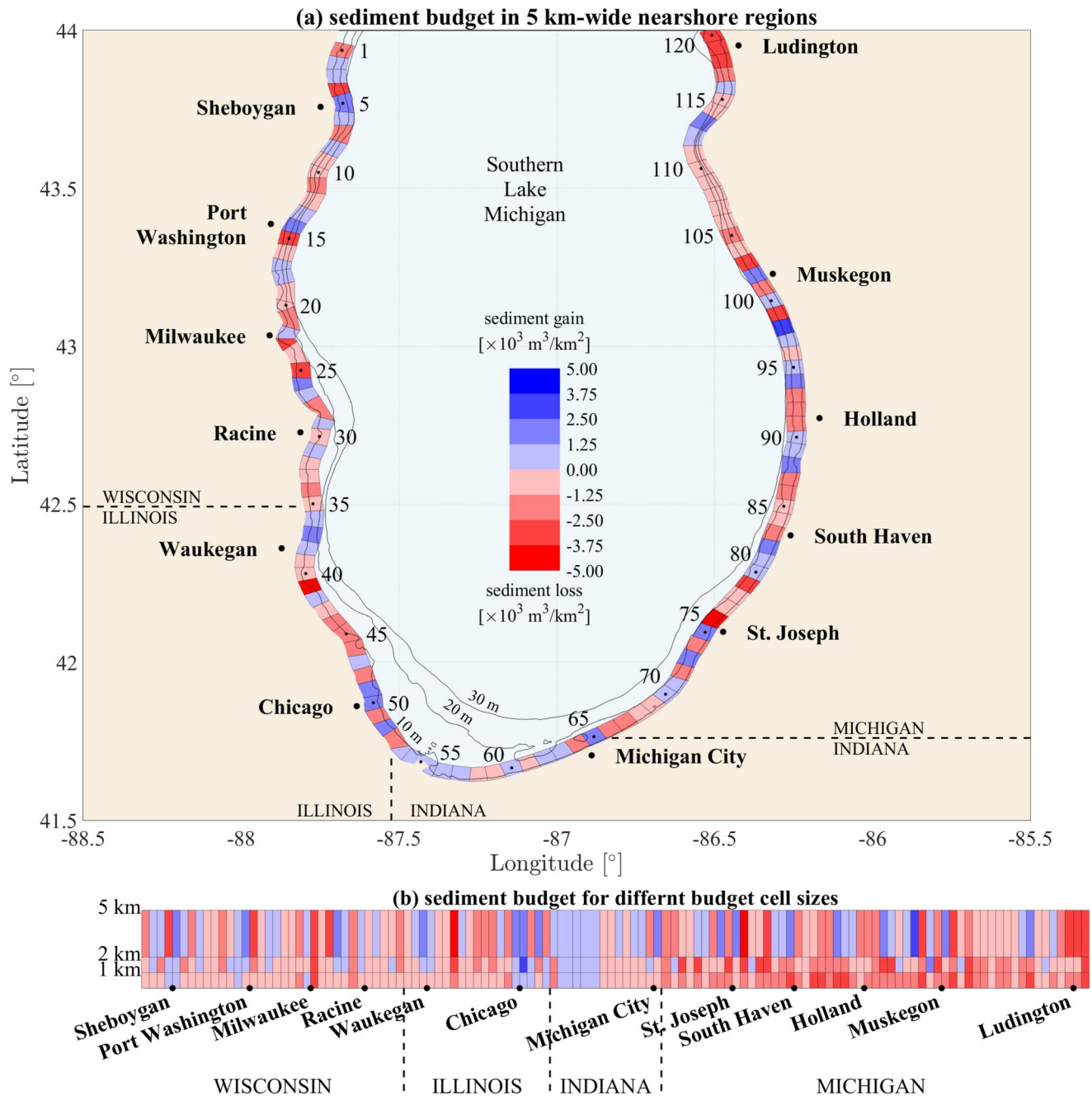


**Figure 9.** (a) The modeled 30-year (1991–2020) mean sediment budget along the ~5 km-wide shore of southern Lake Michigan. The 120 sediment budget cells are about ~5 km in length along the shore. (b) Comparison of the sediment budget in different sized budget cells (1, 2, and 5 km offshore).

cells along southern Wisconsin to the south of Port Washington were dominated by sediment loss. In the southwestern portion of the lake, most budget cells along the shore of Illinois predominantly exhibited sediment loss except for the scattered cells around Waukegan and Chicago, which saw sediment gain. In the southernmost Lake Michigan along the shore of Indiana, most budget cells gained sediment. The sediment deposition pattern in the southwestern and southernmost lake is also consistent with the model results in Khazaei (2020), although this only reflects the period from May to October 2018. The budget cells experienced significant variations in sediment loss or gain along the southeastern shore of Lake Michigan up to Muskegon, MI. In the eastern lake, the budget cells along the coast between Muskegon and Ludington primarily showed sediment loss. Overall, the coastal region was dominated by erosion, aligning with the short-term results (spanning several months) reported

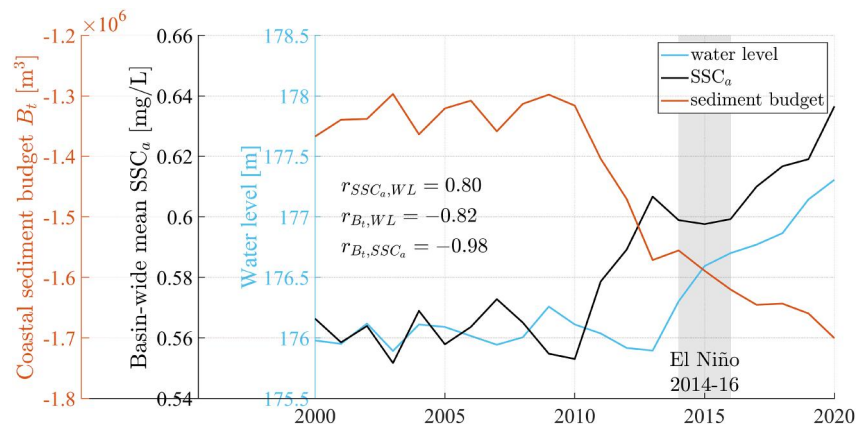


**Figure 10.** Long-term changes of 10-year trailing moving mean coastal sediment budget ( $B_t$ ) and 10-year trailing moving mean basin-wide depth-averaged suspended sediment concentration ( $SSC_a$ ) in southern Lake Michigan as well as the annual water level, where  $B_t$  is the sum of the sediment budget in the 120 budget cells in the 5 km-wide coastal regions (Figure 9a) and negative  $B_t$  indicates sediment loss. The shaded patch indicates the strong El Niño event 2014–16. The correlation coefficients ( $r$ ) among  $B_t$ ,  $SSC_a$ , and water level are shown in the plot.

in Lee et al. (2007) and Khazaei (2020). The total sediment loss averaged over the past 30 years at the erosion cells was  $2.62 \times 10^6 \text{ m}^3$  ( $6.94 \times 10^9 \text{ kg}$ ), of which 44% ( $1.14 \times 10^6 \text{ m}^3$ ,  $3.02 \times 10^9 \text{ kg}$ ) was recouped by the deposition cells alongshore, 8% ( $2.11 \times 10^5 \text{ m}^3$ ,  $0.56 \times 10^9 \text{ kg}$ ) was transported to the northern lake, and 48% ( $1.27 \times 10^6 \text{ m}^3$ ,  $3.37 \times 10^9 \text{ kg}$ ) was transported offshore. This is consistent with the estimation in Lee et al. (2007), which is  $4.05 \times 10^9 \text{ kg}$  per year in the southern basin. The sediment transported offshore, primarily fine sediment, accounted for 75% ( $9.52 \times 10^5 \text{ m}^3$ ,  $2.52 \times 10^9 \text{ kg}$ ). The sediment transported offshore into deep water is presumed to be a “permanent” loss because the sediment is rarely resuspended due to negligible (nearly 0) wave bottom velocities in deep water. The 30-year mean net sediment loss of the entire 5 km-wide coastal water in southern Lake Michigan was  $1.48 \times 10^6 \text{ m}^3$  ( $3.92 \times 10^9 \text{ kg}$ ) including 86% transported offshore and 14% transported to the north.

The comparisons of the sediment budget among different cell sizes (5, 2, and 1 km-wide) are shown in Figure 9b. There are more cells gaining sediment in the 5 km-wide budget cells, while fewer cells gaining sediment in the 2 and 1 km-wide budget cells. One possible explanation is that the sediment suspension is more severe in the areas closer to and within the surf zone, and the suspended sediment may be possibly transported lakeward but partially deposited within the 5 km-wide regions. This phenomenon could result in a 1 km-wide budget cell showing sediment loss while a 5 km-wide budget cell experiences sediment gain (e.g., cell 75 off St. Joseph in Figure 9b).

## 4. Discussion

### 4.1. Temporal and Spatial Characteristics of Coastal Sediment Budget Correlated With SSC

To explore long-term changes in the total sediment budget along the coastal regions ( $B_t$ , sum of the sediment budget in the total 120 budget cells), a 10-year trailing moving mean was applied to remove the seasonal and annual variability (Figure 10 for 5 km-wide coastal regions). Additionally, we analyzed the relationship between the 10-year trailing moving mean of basin-wide depth-averaged SSC (i.e.,  $SSC_a$ ) over the southern lake and the lake water level. The total sediment budget  $B_t$  was negative, signifying sediment loss in the 5 km-wide coastal regions. The larger  $|B_t|$ , the more pronounced the sediment loss. As expected, we observed a strong correlation between total coastal sediment loss ( $|B_t|$ ) and  $SSC_a$  ( $|r_{B_t, SSC_a}| = 0.98$ ). In association with increases in  $SSC_a$ , the total sediment loss ( $|B_t|$ ) also increased dramatically since 2010. Similar to  $SSC_a$ , sediment loss was also highly correlated with water level change with  $|r_{B_t, WL}| = 0.82$  and preceded the water level rise by about 3 years (Figure 10).

While budget cell size may affect the local sediment budget, the trend of the long-term changes in the total sediment budget remains consistent regardless of cell sizes. The total sediment loss in both 2 km-wide and 1 km-wide coastal regions in southern Lake Michigan also accelerated in the past decade (Figures S8 and S9 in Supporting Information S1), in agreement with the result in the 5 km-wide coastal regions (Figure 10).



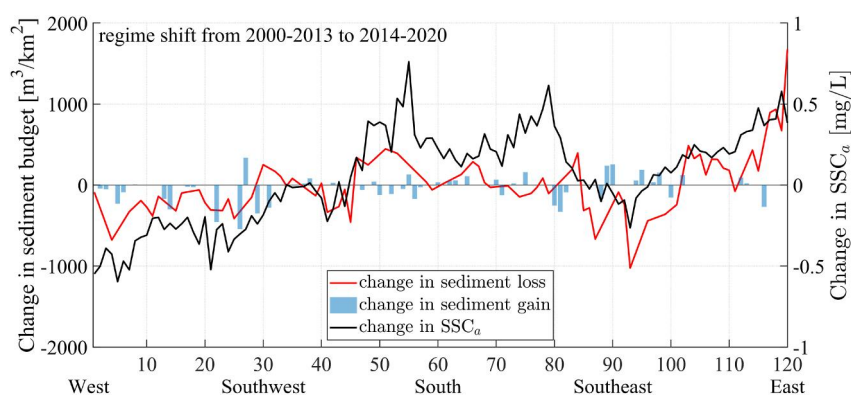


**Figure 11.** The changes in the mean sediment budget (including sediment loss and gain) from 2000 to 2013 with low water levels to 2014–2020 with increasing water levels compared with the changes in depth-averaged suspended sediment concentration ( $SSC_a$ ). The sediment budget is calculated from 120 budget cells in the 5 km-wide coastal regions (Figure 9a) while the  $SSC_a$  is in the middle of the cells about 2.5 km offshore. The correlation coefficient ( $r$ ) between the changes in sediment loss and  $SSC_a$  is 0.57.

After exploring the long-term temporal change in the total coastal sediment budget in southern Lake Michigan, we proceeded to identify the spatial pattern of the local sediment budget. Similar to the local  $SSC_a$ , only a few budget cells exhibit statistically significant ( $p$ -value  $< 0.05$ ) linear trends in sediment budget from 2000 to 2020. Likewise, we conducted a regime shift analysis to examine the spatial pattern of the changes in the local sediment budget from the regime 2000–2013 with low water level to the recent regime 2014–2020 with rapidly increasing water level (Figure 11). The changes in sediment loss between the two regimes correlated with the in  $SSC_a$  changes with a spatial correlation coefficient of  $r = 0.57$ . Consistent with  $SSC_a$ , the sediment changes (loss and gain) decreased (being negative) in the western lake and increased (positive) in the eastern lake. The local sediment gain showed the similar decreasing trend as nearby local sediment loss in the west of the lake, partly due to the fact that the decreasing sediment loss reduces the sediment supply for the sediment gain at nearby cells. Furthermore, the general spatial patterns of the changes in sediment loss (and gain) along the 2 km-wide coastal regions (Figure S10 in Supporting Information S1) are also consistent with the 5 km-wide coastal regions (Figure 11), showing a decreasing trend in the western lake and an increasing trend in the eastern lake.

#### 4.2. Coastal Sediment Budget and Shoreline Changes

We have shown the “coastal sediment budget” that is, sediment loss and gain due to sediment resuspension, transport, and redistribution induced by waves and currents, which can reshape the shoreline over an extended period. In addition to the coastal sediment budget, shoreline changes are also driven by the sediment budget originating from land. This encompasses factors including bluff and shoreline erosion, river influx, and engineering activities such as shoreline armoring and large-scale harbor structures exemplified at St. Joseph. These are not accounted for in the current model due to considerations of computational efficiency. Addressing all the parameters and processes influencing shoreline change requires a suite of models with extremely high resolution (down to  $\sim 1$  m scale and even smaller). Such simulations over a long period (e.g., 30 years) across the entire lake are technically challenging and computationally expensive, thus exceeding the scope of this research. However, as coastal sediment transport is one of the major mechanisms for shoreline change, the long-term change of the coastal sediment budget can still provide valuable information on shoreline change management.

To illustrate the connection between the coastal sediment budget and shoreline change, the sediment budgets (quantified as sediment loss and gain) in budget cells are compared with the historical shoreline changes in Pope et al. (1999) in Figure 12. Although the shoreline changes were computed using historical data from intermittent time periods (10 to over 100 years) before 1991 (Stewart, 1994), our sediment budget generally reflects observed shoreline changes in most cells, showing that the sediment loss (gain) is associated with shoreline recession (accretion). This is particularly evident in the 1 km-wide budget cells (Figure 12a), likely due to the shoreline’s heightened responsiveness to sediment budget changes in the surf zone nearer to the shore. For instance, cells along the shore of southern Wisconsin, predominantly experiencing sediment loss, show a clear association with shoreline recession (Figure 12a). Conversely, sediment gain along the western shore of Indiana is associated with

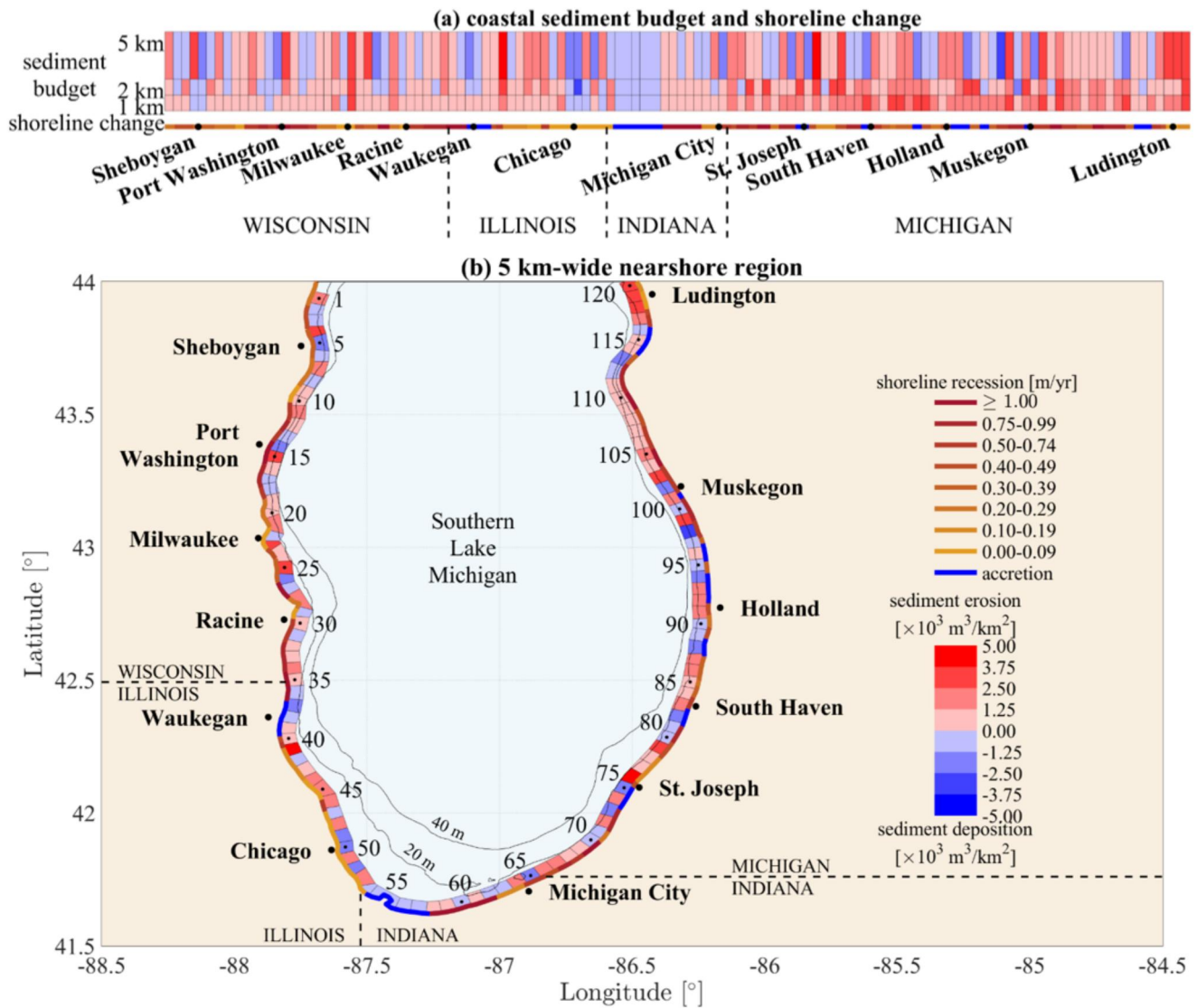


**Figure 12.** (a) The modeled 30-year (1991–2020) mean coastal sediment budget (sediment loss and gain) in the 1, 2, and 5 km-wide budget cells compared with historical shoreline changes in Pope et al. (1999). Note that the shoreline change rate was estimated with historical data (over 10 to more than 100 years) before 1991 (Stewart, 1994). (b) An example of the modeled coastal sediment budget within the 5 km-wide coastal region compared with historical shoreline changes on map.

shoreline accretion. Similarly, the eastern lake exhibits a predominance of sediment loss and consequent shoreline recession with only a few discrepancies. These discrepancies could stem from (a) different time periods for the calculated sediment budget and shoreline changes, and (b) limitations of the present basin-scale model, which neither accounts for the swash zone process nor considers sediment transport from land, or impacts of coastal structures and human activities. Nevertheless, a correlation persists between the coastal sediment budget and shoreline changes. Consequently, the accelerated coastal sediment loss in southern Lake Michigan in the past decade may exacerbate the shoreline erosion, particularly in tandem with lake water level rise. Illustrations of some coastal erosion hotspots in the western and eastern lakes are shown in Figures 13 and 14, respectively. The severe shoreline erosion and bluff collapse have inflicted significant damage to coastal infrastructures and properties.

As mentioned before, owing to model simplification and data limitations, the sediment input from tributaries was not incorporated. Nevertheless, more than half of the input sediment is deposited in deep water (Buckler & Winters, 1983), and the remainder is spatially redistributed through wave-current processes, culminating in a comparable spatial pattern of the resuspended sediment. Therefore, omitting the sediment input is unlikely





**Figure 13.** Illustration of a coastal erosion hotspot in Wisconsin along the coast of the western lake. (a) Location of the hotspot. (b) Historical satellite images (Sources: Google Earth). (c) Historical oblique photos (Sources: <https://www.arcgis.com/home/item.html?id=8cafb47224274bf394e3f2f05a165842>; Credits: Association of State Floodplain Managers Flood Science Center).

significantly alter the overall spatiotemporal pattern of sediment suspension and budget at the basin scale, though it may lead to underestimation of the sediment concentration, especially at the local sites of sediment influx. Additionally, coastal engineering structures were not resolved due to their relatively small dimensions compared to the mesh resolution. The effects of coastal engineering structures could be significant at local sites and play a critical role in local sediment suspension and transport. However, due to their small dimensions, the coastal engineering structures are unlikely to significantly alter the general spatial pattern of the sediment suspension and budget at the basin scale.

The coupled SWAN-FVCOM-CSTMS model effectively simulated physical processes in a broad nearshore region, as corroborated by the measured wave, currents, and SSC data. The model exhibits exceptional performance in basin-scale analysis. The findings indicate that the rate of coastal sediment loss accelerated in response to strengthened winds and wave energy associated with water level rise in the last decade. A recent study by (Kayastha et al., 2022), utilizing the Great Lakes-Atmosphere Regional Model (GLARM), projects that Lake Michigan's average annual water level could rise by 0.44 m by 2040–2049, compared to the 2010–2019 average. The strong correlation observed between coastal sediment loss and water level rise suggests that coastal erosion will also intensify in the coming years. Furthermore, due to climate change, there has been a general decline in winter ice cover across the Great Lakes since 1973, both in terms of maximum extent and duration (Assel





**Figure 14.** Illustration of two coastal erosion hotspots in Michigan along the coast of the eastern lake. (a) Location of the hotspots (b, c). (b, c) Historical satellite images (Sources: Google Earth).

et al., 2003; Wang et al., 2012). This trend of reduced ice coverage and shortened ice duration is projected to persist (Mason et al., 2016; USGCRP, 2017; Wang et al., 2012), driven by regional warming (Xue et al., 2022; Zhang et al., 2020). Consequently, the coastal areas will face greater exposure to intensified wave action during winter seasons (Huang, Zhu, et al., 2021), leading to more severe erosion (Barnes et al., 1994). Therefore, developing adaptation and mitigation strategies for coastal protection is imperative. These strategies should address ongoing lake-level fluctuations and projected regional climate impacts through both conventional hard engineering structures and cost-effective, sustainable, nature-based solutions (Temmerman et al., 2013; Zhu et al., 2020).

## 5. Conclusions

In this study, the coastal sediment transport and budget in southern Lake Michigan from 1991 to 2020 were simulated using coupled SWAN-FVCOM-CSTMS. To the best of our knowledge, this is the first effort in using a coupled wave-current-sediment model for multi-decadal, long-term simulation to analyze the basin-wide coastal sediment budget in the Great Lakes. The results showed that in southern Lake Michigan, the basin-wide mean SSC increased and the coastal sediment loss accelerated, corresponding with intensified wind, current speed, and wave energy, as well as rising lake water levels over the past decade. The strong correlations among these variables reflect the impacts of regional climate on Lake Michigan. Spatially, our results reveal decreased coastal SSC and sediment loss in the western portion of the southern basin, contrasting with an increase in coastal SSC and sediment loss in its eastern sectors. This contrast mirrors a clear shift in the wave climate and hydrodynamic environment. The alterations in long-term coastal sediment budgets imply that considerable shoreline transformations are being influenced by modifications in the wave climate. The projected rise in water levels and diminishing ice coverage and duration in the Great Lakes due to climate change are expected to enhance wave



energy and SSC, resulting in more substantial coastal sediment loss and erosion. It is crucial to comprehend the spatial and temporal dynamics of SSC and coastal sediment budgets for effective water resource management strategies and informed planning of coastal infrastructure.

### Data Availability Statement

The code for FVCOM with built-in CSTMS is available through <https://github.com/FVCOM-GitHub>. The code for SWAN is available through <https://swanmodel.sourceforge.io/download/download.htm>. The bathymetry data sets for Lake Michigan is available through <https://www.ngdc.noaa.gov/mgg/greatlakes/michigan.html>. The CFSR data is available through <https://rda.ucar.edu/datasets/ds093.1>. The CFSv2 data is available through <https://rda.ucar.edu/datasets/ds094.1>.

### Acknowledgments

This is the contribution no. 120 of the Great Lakes Research Center at Michigan Technological University. The Michigan Tech high performance computing cluster, *Superior*, was used in obtaining the modeling results presented in this publication. This work is sponsored by the Michigan Sea Grant College Program, Project Number Index R/SD-5, under award NA18OAR4170102 from National Sea Grant, NOAA, U.S. Department of Commerce, with funds from the State of Michigan. This project is sponsored by the University of Wisconsin Sea Grant Program, under award number NA18OAR4170097. This project is sponsored by the Illinois-Indiana Sea Grant College Program, under award number NA18OAR4170082. This project is also partly supported by the U.S. Department of Energy, Office of Science, under award number DE-SC0024446. Hydrodynamic modeling is also supported by COMPASS-GLM, a multi-institutional project supported by the U.S. Department of Energy, Office of Biological and Environmental Research, Earth and Environmental Systems Modeling program. Hydrodynamic modeling is also supported by the Great Lakes Restoration Initiative, through the University of Michigan Cooperative Institute for Great Lakes Research (CIGLR) cooperative agreement with the (NA17OAR4320152). Hydrodynamic modeling is also supported by the National Aeronautics and Space Administration, Grant 80NSSC17K0287. The hydrodynamic work is also supported by Cooperative Agreement No. G21AC10141 from the United States Geological Survey. The statements, findings, conclusions, and recommendations of authors expressed herein do not necessarily state or reflect those of the United States Government or any agency thereof.

### References

Amoudry, L. O., & Souza, A. J. (2011). Deterministic coastal morphological and sediment transport modeling: A review and discussion. *Reviews of Geophysics*, 49(2), RG2002. <https://doi.org/10.1029/2010RG000341>

Anderson, J. D., Wu, C. H., & Schwab, D. J. (2015). Wave climatology in the apostle islands, lake superior. *Journal of Geophysical Research: Oceans*, 120(7), 4869–4890. <https://doi.org/10.1002/2014JC010278>

Assel, R., Cronk, K., & Norton, D. (2003). Recent trends in Laurentian Great Lakes ice cover. *Climatic Change*, 57(1–2), 185–204. <https://doi.org/10.1023/A:1022140604052>

Barnes, P. W., Kempema, E. W., Reimnitz, E., & McCormick, M. (1994). The influence of ice on Southern Lake Michigan coastal erosion. *Journal of Great Lakes Research*, 20(1), 179–195. [https://doi.org/10.1016/S0380-1330\(94\)71139-4](https://doi.org/10.1016/S0380-1330(94)71139-4)

Berry, W., Rubinstein, N., Melzian, B., & Hill, B. (2003). *The biological effects of suspended and bedded sediment (SABS) in aquatic systems: A review*. United States Environmental Protection Agency. Retrieved from <https://archive.epa.gov/epa/sites/production/files/2015-10/documents/sediment-appendix1.pdf>

Blom, G., van Duin, E. H. S., & Lijklema, L. (1994). Sediment resuspension and light conditions in some shallow Dutch lakes. *Water Science and Technology*, 30(10), 243–252. <https://doi.org/10.2166/wst.1994.0534>

Booij, N., Ris, R. C., & Holthuijsen, L. H. (1999). A third-generation wave model for coastal regions 1. Model description and validation. *Journal of Geophysical Research*, 104(C4), 7649–7666. <https://doi.org/10.1029/98JC02622>

Bozorg-Haddad, O., Delpasand, M., & Loáiciga, H. A. (2021). Water quality, hygiene, and health. In *Economical, political, and social issues in water resources* (pp. 217–257). Elsevier. <https://doi.org/10.1016/B978-0-323-90567-1.00008-5>

Brooks, A. S., & Edgington, D. N. (1994). Biogeochemical control of phosphorus cycling and primary production in Lake Michigan. *Limnology & Oceanography*, 39(4), 961–968. <https://doi.org/10.4319/lo.1994.39.4.0961>

Buckler, W. R., & Winters, H. A. (1983). Lake Michigan bluff recession. *Annals of the Association of American Geographers*, 73(1), 89–110. <https://doi.org/10.1111/j.1467-8306.1983.tb01398.x>

Cardenas, M. P., Schwab, D. J., Eadie, B. J., Hawley, N., & Lesht, B. M. (2005). Sediment transport model validation in Lake Michigan. *Journal of Great Lakes Research*, 31(4), 373–385. [https://doi.org/10.1016/S0380-1330\(05\)70269-0](https://doi.org/10.1016/S0380-1330(05)70269-0)

Changnon, S. A., Jr. (1987). Climate fluctuations and record-high levels of Lake Michigan. *Bulletin of the American Meteorological Society*, 68(11), 1394–1402. [https://doi.org/10.1175/1520-0477\(1987\)068<1394:cfarhl>2.0.co;2](https://doi.org/10.1175/1520-0477(1987)068<1394:cfarhl>2.0.co;2)

Chen, C., Beardsley, R., & Cowles, G. (2006). An unstructured grid, finite-volume coastal ocean model (FVCOM) system. *Oceanography*, 19(1), 78–89. <https://doi.org/10.5670/oceanog.2006.92>

Chen, C., Liu, H., & Beardsley, R. C. (2003). An unstructured grid, finite-volume, three-dimensional, primitive equations ocean model: Application to coastal ocean and estuaries. *Journal of Atmospheric and Oceanic Technology*, 20(1), 159–186. [https://doi.org/10.1175/1520-0426\(2003\)020<0159:AUGFVT>2.0.CO;2](https://doi.org/10.1175/1520-0426(2003)020<0159:AUGFVT>2.0.CO;2)

Chen, C., Wang, L., Ji, R., Budd, J. W., Schwab, D. J., Beletsky, D., et al. (2004). Impacts of suspended sediment on the ecosystem in Lake Michigan: A comparison between the 1998 and 1999 plume events. *Journal of Geophysical Research*, 109(10), 1–18. <https://doi.org/10.1029/2002JC001687>

Cheng, T. K., Hill, D. F., Beamer, J., & Garcia-Medina, G. (2015). Climate change impacts on wave and surge processes in a Pacific Northwest (USA) estuary. *Journal of Geophysical Research: Oceans*, 120(1), 182–200. <https://doi.org/10.1002/2014JC010268>

Colman, S. M., & Foster, D. S. (1994). A sediment budget for southern Lake Michigan: Source and sink models for different time intervals. *Journal of Great Lakes Research*, 20(1), 215–228. [https://doi.org/10.1016/S0380-1330\(94\)71142-4](https://doi.org/10.1016/S0380-1330(94)71142-4)

Deacu, D., Fortin, V., Klyszajko, E., Spence, C., & Blanken, P. D. (2012). Predicting the net basin supply to the Great Lakes with a hydro-meteorological model. *Journal of Hydrometeorology*, 13(6), 1739–1759. <https://doi.org/10.1175/JHM-D-11-0151.1>

Dietrich, J. C., Westerink, J. J., Kennedy, A. B., Smith, J. M., Jensen, R. E., Zijlema, M., et al. (2011). Hurricane Gustav (2008) waves and storm surge: Hindcast, synoptic analysis, and validation in Southern Louisiana. *Monthly Weather Review*, 139(8), 2488–2522. <https://doi.org/10.1175/2011MWR3611.1>

Donelan, M. A., Hui, W. H., & Hamilton, J. (1985). Directional spectra of wind-generated ocean waves. *Philosophical Transactions of the Royal Society of London - Series A: Mathematical and Physical Sciences*, 315(1534), 509–562. <https://doi.org/10.1098/rsta.1985.0054>

Eadie, B., & Lozano, S. (1999). Grain size distribution of the surface sediments collected during the Lake Michigan mass balance and environmental mapping and assessment programs. In *NOAA technical memorandum ERL GLERL*. Retrieved from [https://repository.library.noaa.gov/view/noaa/11132/noaa\\_11132\\_DS1.pdf](https://repository.library.noaa.gov/view/noaa/11132/noaa_11132_DS1.pdf)

Eadie, B. J., Chambers, R. L., Gardner, W. S., & Bell, G. L. (1984). Sediment trap studies in Lake Michigan: Resuspension and chemical fluxes in the southern basin. *Journal of Great Lakes Research*, 10(3), 307–321. [https://doi.org/10.1016/S0380-1330\(84\)71844-2](https://doi.org/10.1016/S0380-1330(84)71844-2)

Eadie, B. J., & Robbins, J. A. (1987). The role of particulate matter in the movement of contaminants in the great lakes. In *Sources and fates of aquatic pollutants* (pp. 319–364). Advances in Chemistry. <https://doi.org/10.1021/ba-1987-0216.ch011>

Eadie, B. J., Robbins, J. A., Val Klump, J., Schwab, D. J., & Edgington, D. N. (2008). Winter-spring storms and their influence on sediment resuspension, transport, and accumulation patterns in southern Lake Michigan. *Oceanography*, 21(4), 118–135. <https://doi.org/10.5670/oceanog.2008.09>

- Eadie, B. J., Schwab, D. J., Assel, R. A., Hawley, N., Lansing, M. B., Miller, G. S., et al. (1996). Development of recurrent coastal plume in Lake Michigan observed for first time. *Eos, Transactions American Geophysical Union*, 77(35), 337–338. <https://doi.org/10.1029/96EO00234>
- Eadie, B. J., Schwab, D. J., Johengen, T. H., Lavrentyev, P. J., Miller, G. S., Holland, R. E., et al. (2002). Particle transport, nutrient cycling, and algal community structure associated with a major winter-spring sediment resuspension event in Southern Lake Michigan. *Journal of Great Lakes Research*, 28(3), 324–337. [https://doi.org/10.1016/S0380-1330\(02\)70588-1](https://doi.org/10.1016/S0380-1330(02)70588-1)
- Gao, G. D., Wang, X. H., Song, D., Bao, X., Yin, B. S., Yang, D. Z., et al. (2018). Effects of wave–current interactions on suspended-sediment dynamics during strong wave events in Jiaozhou Bay, Qingdao, China. *Journal of Physical Oceanography*, 48(5), 1053–1078. <https://doi.org/10.1175/JPO-D-17-0259.1>
- Ge, J., Zhou, Z., Yang, W., Ding, P., Chen, C., Wang, Z. B., & Gu, J. (2018). Formation of concentrated benthic suspension in a time-dependent salt wedge estuary. *Journal of Geophysical Research: Oceans*, 123(11), 8581–8607. <https://doi.org/10.1029/2018JC013876>
- Grant, W. D., & Madsen, O. S. (1979). Combined wave and current interaction with a rough bottom. *Journal of Geophysical Research*, 84(C4), 1797–1808. <https://doi.org/10.1029/JC084iC04p01797>
- Gronewold, A. D., Do, H. X., Mei, Y., & Stow, C. A. (2021). A tug-of-war within the hydrologic cycle of a continental freshwater basin. *Geophysical Research Letters*, 48(4), 1–8. <https://doi.org/10.1029/2020GL090374>
- Gronewold, A. D., & Rood, R. B. (2019). Recent water level changes across Earth's largest lake system and implications for future variability. *Journal of Great Lakes Research*, 45(1), 1–3. <https://doi.org/10.1016/j.jglr.2018.10.012>
- Hawley, N., Harris, C. K., Lesht, B. M., & Clites, A. H. (2009). Sensitivity of a sediment transport model for Lake Michigan. *Journal of Great Lakes Research*, 35(4), 560–576. <https://doi.org/10.1016/j.jglr.2009.06.004>
- Hawley, N., & Lee, C.-H. (1999). Sediment resuspension and transport in Lake Michigan during the unstratified period. *Sedimentology*, 46(5), 791–805. <https://doi.org/10.1046/j.1365-3091.1999.00251.x>
- Huang, C., Anderson, E., Liu, Y., Ma, G., Mann, G., & Xue, P. (2021). Evaluating essential processes and forecast requirements for meteotsunami-induced coastal flooding. *Natural Hazards*, 110(3), 1693–1718. <https://doi.org/10.1007/s11069-021-05007-x>
- Huang, C., Zhu, L., Ma, G., Meadows, G. A., & Xue, P. (2021). Wave climate associated with changing water level and ice cover in Lake Michigan. *Frontiers in Marine Science*, 8(November), 1–18. <https://doi.org/10.3389/fmars.2021.746916>
- Huang, Y., Weisberg, R. H., Zheng, L., & Zijlema, M. (2013). Gulf of Mexico hurricane wave simulations using SWAN: Bulk formula-based drag coefficient sensitivity for Hurricane Ike. *Journal of Geophysical Research: Oceans*, 118(8), 3916–3938. <https://doi.org/10.1002/jgrc.20283>
- Jensen, R. E., Cialone, M. A., Chapman, R. S., Ebersole, B. A., Anderson, M., & Thomas, L. (2012). Lake Michigan storm: Wave and water level modeling engineer research and development. In *ERDC/CHL TR-12-26*. (Issue May).
- Ji, R., Chen, C., Budd, J. W., Schwab, D. J., Beletsky, D., Fahnenstiel, G. L., et al. (2002). Influences of suspended sediments on the ecosystem in Lake Michigan: A 3-D coupled bio-physical modeling experiment. *Ecological Modelling*, 152(2–3), 169–190. [https://doi.org/10.1016/S0304-3800\(02\)00027-3](https://doi.org/10.1016/S0304-3800(02)00027-3)
- Kayastha, M. B., Ye, X., Huang, C., & Xue, P. (2022). Future rise of the Great Lakes water levels under climate change. *Journal of Hydrology*, 612, 128205. <https://doi.org/10.1016/j.jhydrol.2022.128205>
- Khazaei, B. (2020). *Development of a hydrodynamic and sediment transport model for Green Bay*. University of Wisconsin-Milwaukee. Retrieved from <https://dc.uwm.edu/etd/2392/>
- Khazaei, B., Bravo, H. R., Anderson, E. J., & Klump, J. V. (2021). Development of a physically based sediment transport model for Green Bay, Lake Michigan. *Journal of Geophysical Research: Oceans*, 126(10). <https://doi.org/10.1029/2021jc017518>
- Lee, C., Schwab, D. J., Beletsky, D., Stroud, J., & Lesht, B. (2007). Numerical modeling of mixed sediment resuspension, transport, and deposition during the March 1998 episodic events in southern Lake Michigan. *Journal of Geophysical Research*, 112(C2), C02018. <https://doi.org/10.1029/2005JC003419>
- Lee, C., Schwab, D. J., & Hawley, N. (2005). Sensitivity analysis of sediment resuspension parameters in coastal area of southern Lake Michigan. *Journal of Geophysical Research*, 110(C3), 1–16. <https://doi.org/10.1029/2004JC002326>
- Li, S., Ji, C., Zhang, Q., & Chen, T. (2022). Numerical simulations of coastal overwash using A phase-averaged wave—current—sediment transport model. *China Ocean Engineering*, 36(2), 191–207. <https://doi.org/10.1007/s13344-022-0015-x>
- Lou, J., Schwab, D. J., Beletsky, D., & Hawley, N. (2000). A model of sediment resuspension and transport dynamics in southern Lake Michigan. *Journal of Geophysical Research*, 105(C3), 6591–6610. <https://doi.org/10.1029/1999JC900325>
- Mao, M., van der Westhuysen, A. J., Xia, M., Schwab, D. J., & Chawla, A. (2016). Modeling wind waves from deep to shallow waters in Lake Michigan using unstructured SWAN. *Journal of Geophysical Research: Oceans*, 121(6), 3836–3865. <https://doi.org/10.1002/2015JC011340>
- Mao, M., & Xia, M. (2017). Dynamics of wave–current–surge interactions in Lake Michigan: A model comparison. *Ocean Modelling*, 110, 1–20. <https://doi.org/10.1016/j.oceomod.2016.12.007>
- Mason, L. A., Riseng, C. M., Gronewold, A. D., Rutherford, E. S., Wang, J., Clites, A., et al. (2016). Fine-scale spatial variation in ice cover and surface temperature trends across the surface of the Laurentian Great Lakes. *Climatic Change*, 138(1–2), 71–83. <https://doi.org/10.1007/s10584-016-1721-2>
- Meadows, G. A., Meadows, L. A., Wood, W. L., Hubertz, J. M., & Perlin, M. (1997). The relationship between great lakes water levels, wave energies, and shoreline damage. *Bulletin of the American Meteorological Society*, 78(4), 675–682. [https://doi.org/10.1175/1520-0477\(1997\)078<0675:TRBGLW>2.0.CO;2](https://doi.org/10.1175/1520-0477(1997)078<0675:TRBGLW>2.0.CO;2)
- Mei, C. C., Fan, S. J., & Jin, K. R. (1997). Resuspension and transport of fine sediments by waves. *Journal of Geophysical Research*, 102(C7), 15807–15821. <https://doi.org/10.1029/97JC00584>
- Mellor, G. L., & Yamada, T. (1982). Development of a turbulence closure model for geophysical fluid problems. *Reviews of Geophysics and Space Physics*, 20(4), 851–875. <https://doi.org/10.1029/RG020i004p00851>
- Miles, T., Glenn, S. M., & Schofield, O. (2013). Temporal and spatial variability in fall storm induced sediment resuspension on the Mid-Atlantic Bight. *Continental Shelf Research*, 63, S36–S49. <https://doi.org/10.1016/j.csr.2012.08.006>
- Miller, D. H., Xia, X., Huang, W.-C., & Rossmann, R. (2016). Distribution of sediment measurements in Lake Michigan as a case study: Implications for estimating sediment and water interactions in eutrophication and bioaccumulation models. *Applied Mathematics*, 07(15), 1846–1867. <https://doi.org/10.4236/am.2016.715153>
- Millie, D. F., Fahnenstiel, G. L., Carrick, H. J., Lohrenz, S. L., & Schofield, O. M. E. (2002). Spatial variation in Lake Michigan phytoplankton composition during sediment resuspension events. *SIL Proceedings, 1922-2010*, 28(3), 1216–1220. <https://doi.org/10.1080/03680770.2001.11902647>
- Mortimer, C. H. (1988). Discoveries and testable hypotheses arising from coastal zone color scanner imagery of southern Lake Michigan I. *Limnology & Oceanography*, 33(2), 203–226. <https://doi.org/10.4319/lo.1988.33.2.0203>
- Niroomandi, A., Ma, G., Ye, X., Lou, S., & Xue, P. (2018). Extreme value analysis of wave climate in Chesapeake Bay. *Ocean Engineering*, 159, 22–36. <https://doi.org/10.1016/j.oceaneng.2018.03.094>

- Niu, Q., Xia, M., Ludsin, S. A., Chu, P. Y., Mason, D. M., & Rutherford, E. S. (2018). High-turbidity events in Western Lake Erie during ice-free cycles: Contributions of river-loaded vs. resuspended sediments. *Limnology & Oceanography*, *63*(6), 2545–2562. <https://doi.org/10.1002/lno.10959>
- Pope, J., Stewart, C. J., Dolan, R., Peatross, J., & Thompson, C. L. (1999). The great lakes shoreline type, erosion and accretion - Public information map sheet. In *United States geological Survey, department of the interior*.
- Pore, N. A. (1979). Automated wave forecasting for the great lakes. *Monthly Weather Review*, *107*(10), 1275–1286. [https://doi.org/10.1175/1520-0493\(1979\)107<1275:AWFFTG>2.0.CO;2](https://doi.org/10.1175/1520-0493(1979)107<1275:AWFFTG>2.0.CO;2)
- Qi, J., Chen, C., Beardsley, R. C., Perrie, W., Cowles, G. W., & Lai, Z. (2009). An unstructured-grid finite-volume surface wave model (FVCOM-SWAVE): Implementation, validations and applications. *Ocean Modelling*, *28*(1–3), 153–166. <https://doi.org/10.1016/j.ocemod.2009.01.007>
- Robbins, J. A., & Eadie, B. J. (1991). Seasonal cycling of trace elements 137 Cs, 7 Be, and 239+240 Pu in Lake Michigan. *Journal of Geophysical Research*, *96*(C9), 17081–17104. <https://doi.org/10.1029/91JC01412>
- Rosati, J. D. (2005). Concepts in sediment budgets. *Journal of Coastal Research*, *212*(2), 307–322. <https://doi.org/10.2112/02-475A.1>
- Saha, S., Moorthi, S., Pan, H.-L., Wu, X., Wang, J., Nadiga, S., et al. (2010). NCEP climate forecast system Reanalysis (CFSR) selected hourly time-series products, January 1979 to December 2010. *Research Data Archive at the National Center for Atmospheric Research, Computational and Information Systems Laboratory*. <https://doi.org/10.5065/D6513W89>
- Saha, S., Moorthi, S., Wu, X., Wang, J., Nadiga, S., Tripp, P., et al. (2011). NCEP climate forecast system version 2 (CFsv2) selected hourly time-series products. *Research Data Archive at the National Center for Atmospheric Research, Computational and Information Systems Laboratory*. <https://doi.org/10.5065/D6N877VB>
- Schwab, D. J., Eadie, B. J., Assel, R. A., & Roebber, P. J. (2006). Climatology of large sediment resuspension events in Southern Lake Michigan. *Journal of Great Lakes Research*, *32*(1), 50–62. [https://doi.org/10.3394/0380-1330\(2006\)32\[50:COLSRE\]2.0.CO;2](https://doi.org/10.3394/0380-1330(2006)32[50:COLSRE]2.0.CO;2)
- Smagorinsky, J. (1963). General circulation experiments with the primitive equations: I. The basic experiment. *Monthly Weather Review*, *91*(3), 99–164. [https://doi.org/10.1175/1520-0493\(1963\)091<0099:GCEWTP>2.3.CO;2](https://doi.org/10.1175/1520-0493(1963)091<0099:GCEWTP>2.3.CO;2)
- Soulsby, R. (1997). *Dynamics of marine sands: A manual for practical applications*. Thomas Telford Publications.
- Stewart, C. J. (1994). United States Great Lakes shoreline recession rate data. Final report for U.S. Army Corps of Engineers. Retrieved from <http://www.cjsgcons.com/downloads/RecREPORT1.pdf>
- Temmerman, S., Meire, P., Bouma, T. J., Herman, P. M. J., Ysebaert, T., & De Vriend, H. J. (2013). Ecosystem-based coastal defence in the face of global change. *Nature*, *504*(7478), 79–83. <https://doi.org/10.1038/nature12859>
- USGCRP. (2017). Climate science special report: Fourth national climate assessment. In D. J. Wuebbles, D. W. Fahey, K. A. Hibbard, D. J. Dokken, B. C. Stewart, et al. (Eds.), *U.S. Global Change Research Program* (Vol. I, p. 470). <https://doi.org/10.7930/J0J964J6>
- Wang, J., Bai, X., Hu, H., Clites, A., Colton, M., & Lofgren, B. (2012). Temporal and spatial variability of Great Lakes ice cover, 1973–2010. *Journal of Climate*, *25*(4), 1318–1329. <https://doi.org/10.1175/2011JCLI4066.1>
- Warner, J. C., Sherwood, C. R., Signell, R. P., Harris, C. K., & Arango, H. G. (2008). Development of a three-dimensional, regional, coupled wave, current, and sediment-transport model. *Computers & Geosciences*, *34*(10), 1284–1306. <https://doi.org/10.1016/j.cageo.2008.02.012>
- Wu, L., Chen, C., Guo, P., Shi, M., Qi, J., & Ge, J. (2011). A FVCOM-based unstructured grid wave, current, sediment transport model, I. Model description and validation. *Journal of Ocean University of China*, *10*(1), 1–8. <https://doi.org/10.1007/s11802-011-1788-3>
- Xie, D., Zou, Q.-P., Mignone, A., & MacRae, J. D. (2019). Coastal flooding from wave overtopping and sea level rise adaptation in the northeastern USA. *Coastal Engineering*, *150*, 39–58. <https://doi.org/10.1016/j.coastaleng.2019.02.001>
- Xie, D., Zou, Q., & Cannon, J. W. (2016). Application of SWAN+ADCIRC to tide-surge and wave simulation in Gulf of Maine during Patriot's Day storm. *Water Science and Engineering*, *9*(1), 33–41. <https://doi.org/10.1016/j.wse.2016.02.003>
- Xue, P., Pal, J. S., Ye, X., Lenters, J. D., Huang, C., & Chu, P. Y. (2017). Improving the simulation of large lakes in regional climate modeling: Two-way lake-atmosphere coupling with a 3D hydrodynamic model of the great lakes. *Journal of Climate*, *30*(5), 1605–1627. <https://doi.org/10.1175/JCLI-D-16-0225.1>
- Xue, P., Schwab, D. J., & Hu, S. (2015). An investigation of the thermal response to meteorological forcing in a hydrodynamic model of Lake Superior. *Journal of Geophysical Research: Oceans*, *120*(7), 5233–5253. <https://doi.org/10.1002/2015JC010740>
- Xue, P., Ye, X., Pal, J. S., Chu, P. Y., Kayastha, M. B., & Huang, C. (2022). Climate projections over the great lakes region: Using two-way coupling of a regional climate model with a 3-D lake model. *Geoscientific Model Development*, *15*(11), 4425–4446. <https://doi.org/10.5194/gmd-15-4425-2022>
- Yang, G., Wang, X. H., Zhong, Y., & Oliver, T. S. N. (2022). Modelling study on the sediment dynamics and the formation of the flood-tide delta near Cullendulla Beach in the Batemans Bay, Australia. *Marine Geology*, *452*(March), 106910. <https://doi.org/10.1016/j.margeo.2022.106910>
- Zhang, L., Zhao, Y., Hein-Griggs, D., Janes, T., Tucker, S., & Ciborowski, J. J. H. (2020). Climate change projections of temperature and precipitation for the great lakes basin using the PRECIS regional climate model. *Journal of Great Lakes Research*, *46*(2), 255–266. <https://doi.org/10.1016/j.jglr.2020.01.013>
- Zhou, Z., Ge, J., van Maren, D. S., Wang, Z. B., Kuai, Y., & Ding, P. (2021). Study of sediment transport in a tidal channel-shoal system: Lateral effects and slack-water dynamics. *Journal of Geophysical Research: Oceans*, *126*(3), 1–23. <https://doi.org/10.1029/2020JC016334>
- Zhu, L., Huguénard, K., Zou, Q., Fredriksson, D. W., & Xie, D. (2020). Aquaculture farms as nature-based coastal protection: Random wave attenuation by suspended and submerged canopies. *Coastal Engineering*, *160*, 103737. <https://doi.org/10.1016/j.coastaleng.2020.103737>